A Mathematical Model for Atrial Fibrillation

by

Ronald David Berger

B.S., Massachusetts Institute of Technology
(1981)

Submitted to the Department of
Electrical Engineering and Computer Science
in Partial Fulfillment of the
Requirements for the Degree of

Master of Science at the

Massachusetts Institute of Technology
September, 1983

Signature of Author.....
Department of Electrical Engineering
August 30, 1983

Certified by .....
Thesis Supervisor

Accepted by .....
Chairman, Departmental Committee on Theses

A Mathematical Model for Atrial Fibrillation

by Ronald David Berger

ABSTRACT

. The principal statistical properties of the RR interval sequence during atrial fibrillation are reviewed. A simple quantitative electrophysiologic model is presented which successfully accounts for these statistical features. In this model the atrioventricular junction (AVJ) is treated as a single cell equivalent characterized by a refractory period and spontaneous rate of phase four depolarization. The atria are presumed to bombard the AVJ with impulses that arrive randomly in time; each impulse induces a partial depolarization of the AVJ equivalent cell. It is then shown that other models for the ventricular response during atrial fibrillation (*e.g.* concealed conduction models) do not adequately account for the salient statistical features of the RR interval sequence. The present model may be utilized to characterize a sequence of RR intervals recorded from a given individual in terms of the numerical magnitudes of the model's four parameters: the mean rate at which atrial impulses bombard the AVJ, the relative amplitude of the impulses, the relative rate of spontaneous phase four depolarization of the AVJ equivalent cell, and the refractory period of the AVJ equivalent cell. Such a characterization may be useful in studying mechanisms of drug action and interaction, as well as potentially offering a quantitative means for optimizing pharmacologic management of chronic atrial fibrillation.

Thesis Supervisor: Dr. Richard J. Cohen

Title: Associate Professor of Health Sciences and Technology
and of Physics

Acknowledgement

The author would like to express his gratitude to Prof. Richard Cohen who developed and supervised this research project, for providing the careful guidance and mathematical ingenuity that were frequently required during the course of the project; to the other members of Prof. Cohen's laboratory, especially Robert Kenet, Solange Akselrod, and Michael Bailin, for all they have taught him about physiology, engineering, and experimental technique; and to Cory Myers for his assistance in the text formatting required to print this thesis.

The author is also grateful for the continuing moral support provided by his parents, Mr. and Mrs. Joseph Berger, and by his friends, especially Linda Brafman.

Table of Contents

List of Figures

Chapter 1

Introduction

The 'irregularly irregular' pulse has long been recognized as the clinical hallmark of the dysrhythmia, atrial fibrillation. A more precise characterization of the ventricular interbeat interval (RR interval) variability during atrial fibrillation may be obtained by statistical analysis of the sequence of RR intervals measured from the surface electrocardiogram.

A simple, yet quantitative, model for the genesis of RR interval fluctuations during atrial fibrillation is presented in this thesis. The model is based upon well known clinical electrophysiological observations. The predictions of this model are compared with the known statistical properties of the RR interval sequences during atrial fibrillation, and are shown, in fact, to account for all the principal statistical properties. Also considered are other existing models for the source of the RR interval variability (*e.g.* concealed conduction models), and these are shown to lack the ability to similarly account for these statistical features.

Finally, in this thesis it is shown how one can apply the model to the analysis of atrial fibrillation in a given individual. From a sequence of 1000 successive RR intervals, one may deduce the numerical magnitudes of the model's four electrophysiologic parameters. In this fashion one may evaluate the response to pharmacologic agents in terms of changes in the magnitudes of the model's parameters.

Chapter 2

Statistical Properties of RR Interval Fluctuations

The analysis begins by contrasting the statistical properties of the RR interval fluctuations during normal sinus rhythm with the RR interval fluctuations during atrial fibrillation. The RR interval fluctuates during normal sinus rhythm primarily in response to the extrinsic autonomic nervous system's modulation of the activity of the sinoatrial node and the cardiac conduction system [1]. Such modulation plays an important role in short-term cardiovascular regulation in the face of perturbations due to respiratory activity, adjustments in resistance to flow in various vascular beds, changes in posture, etc. On the other hand, during atrial fibrillation the RR interval fluctuations reflect primarily the intrinsic variability of the conduction processes which sustain the dysrhythmia. (However, effects of autonomic modulation may be superimposed on this intrinsic variability [6,7].)

Given the very different physiologic sources of RR interval variability during normal sinus rhythm and atrial fibrillation, it is not surprising that the statistical properties of the RR interval sequence should differ significantly between the two rhythms. The RR interval histogram is considered first, followed by a look at the autocovariance function.

§2.1 RR Interval Histogram

During normal sinus rhythm the RR interval histogram is often Gaussian in shape [11] (see Figure 2.1), and the standard deviation σ is usually small compared to the mean RR interval $\bar{T}$. Typically, the coefficient of variation, $\sigma/\bar{T}$, is on the order of 0.05 to 0.08 in resting adults. On the other hand, during atrial fibrillation the RR interval histogram is generally much broader with $\sigma/\bar{T}$ greater than 0.2 [3,17]. Moreover, the shape of the histogram is much more variable. The distribution may be unimodal with a single smooth peak as shown in Figure 2.2a, or it may have a single narrow peak superimposed on a smooth background as shown in Figure 2.3a, or it may be charac-

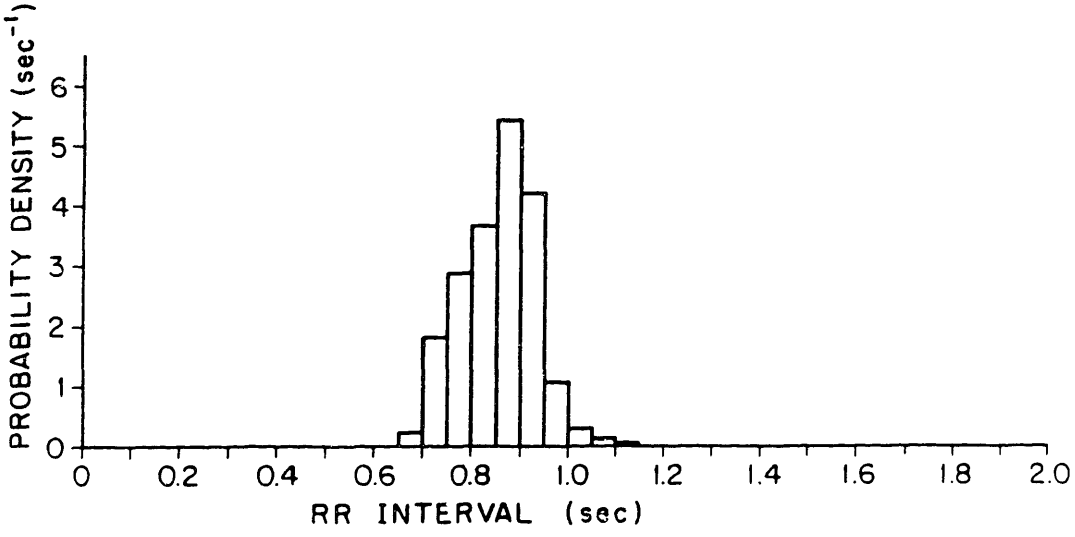

Figure 2.1: Typical RR interval histogram during normal sinus rhythm in resting man.

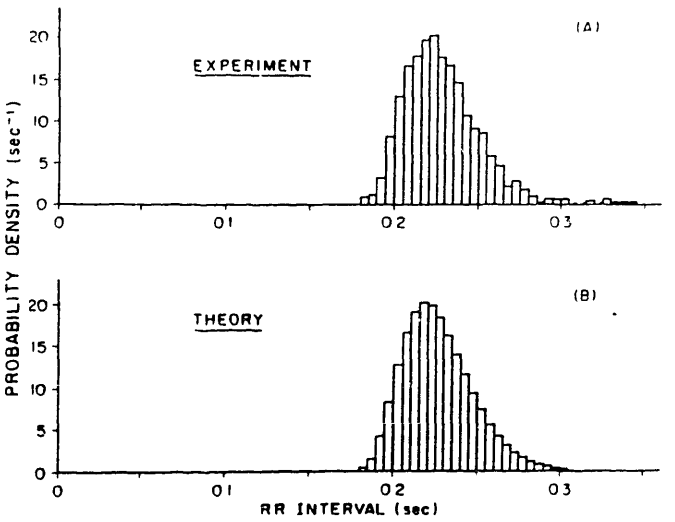

Figure 2.2: (A) Unimodal RR interval histogram obtained from ECG of anesthetized dog in which atrial fibrillation was electrically induced with 60Hz current source. (B) Theoretical histogram predicted by model representing best-fit to experimental histogram shown in (A). The deduced model parameters are: $\lambda = 116/\text{sec}$, $\tau = 0.175$ sec, $0.167 < \Delta V/(V_T - V_R) < 0.2$, and $0 < \dot{V}_4/(V_T - V_R) < 1.07/\text{sec}$.

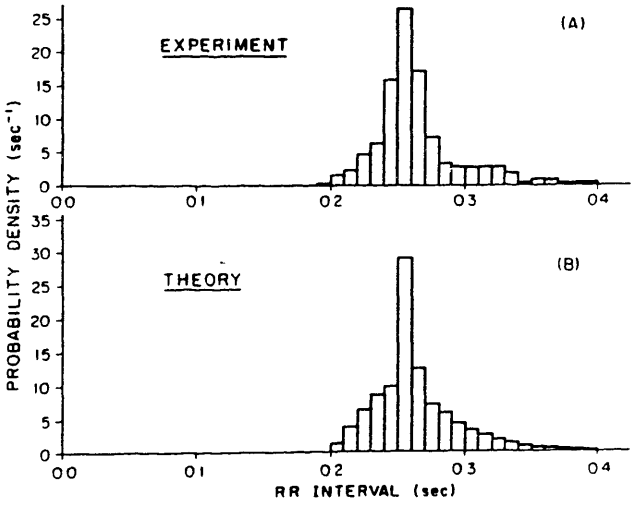

Figure 2.3: (A) RR interval histogram obtained during electrically induced atrial fibrillation in anesthetized dog. (B) Best-fit theoretical histogram corresponding to experimental histogram shown in (A). $\lambda = 46.2/\text{sec}$, $\tau = 0.191$ sec, $0.285 < \Delta V/(V_T - V_R) < 0.333$, and $0 < \dot{V}_4/(V_T - V_R) < 2.20/\text{sec}$. Note the presence of a single delta function superimposed on pieces from two Erlang curves. The delta function is represented as having an intrinsic width of one bin, so its area is distributed between two adjacent bins in a ratio determined by the location of the center of the delta function.

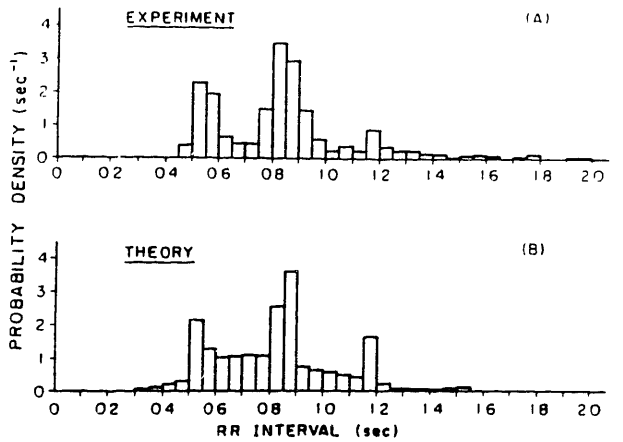

Figure 2.4: (A) RR interval histogram from patient E.A. in chronic atrial fibrillation. Note the presence of several evenly spaced peaks. (B) Best-fit theoretical histogram corresponding to histogram shown in (A). $\lambda = 4.88$/sec, $\tau = 0.117$ sec, $\Delta V/(V_T - V_R) = 0.189$, and $\dot{V}_4/(V_T - V_R) = 0.585$/sec. Each delta function is presumed to have an intrinsic width of one bin as discussed in Figure 2.3.

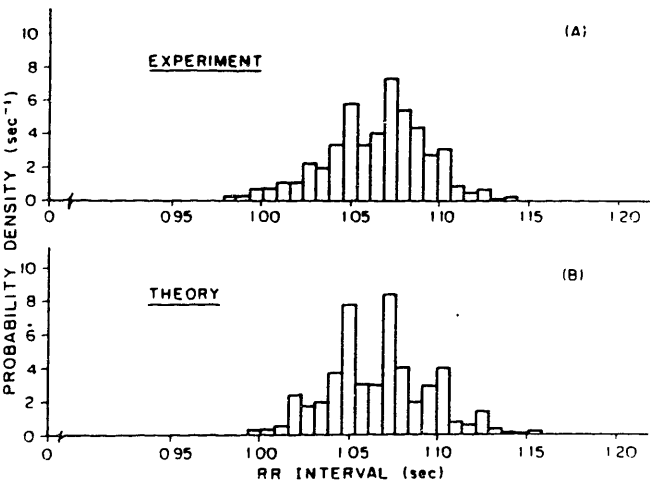

Figure 2.5: (A) RR interval histogram from patient L.B. in chronic atrial fibrillation. The closely spaced peaks seen in this histogram are barely resolvable into individual peaks by the algorithm to deduce the model parameters. (B) Best-fit theoretical histogram corresponding to histogram shown in (A). $\lambda = 50$/sec, $\tau = 0.935$ sec, $\Delta V/(V_T - V_R) = 0.088$, and $\dot{V}_4/(V_T - V_R) = 3.40$/sec. Each delta function is represented as having an intrinsic width of one bin as discussed in Figure 2.3.

terized by multiple peaks as shown in Figure 2.4a [2,4,10,12,16]. Indeed Arnoldi [2] and Söderström [16] noted that the general form of the histogram is that of a smooth distribution upon which is superimposed a set of evenly spaced narrow peaks (as shown in Figure 2.4a). Söderström typically observed such peaks in patients at RR intervals of 0.35. 0.70, 1.05, and 1.40 seconds. He noted that even when multiple peaks were not evident in a histogram, they often could be brought out by changing mean ventricular rate by drug administration or exercise. He inferred that multiple peaks were always present in the histogram, but might not be detected because of low amplitude.

§2.2 Autocovariance Function of RR Interval Sequence

The RR interval histogram contains information on the relative frequency of occurrence of RR intervals of different lengths, but contains no information on the correlation between the length of one RR interval and subsequent RR intervals. To characterize this feature of the RR interval sequence, one may compute the serial autocovariance coefficients, R_i, of the RR interval sequence:

$$R_i = \frac{1}{(\bar{T})^2(N-i-1)} \sum_{j=0}^{N-i-1} (T_{i+j} - \bar{T})(T_j - \bar{T}) \tag{2.1}$$

where

$$\bar{T} = \frac{1}{N} \sum_{j=0}^{N-1} T_j \tag{2.2}$$

Here N denotes the number of RR intervals in the sequence (typically N is on the order of 1,000); $\bar{T}$ is the mean RR interval. Each coefficient R_i denotes the degree of correlation between one RR interval and the RR interval occurring i beats later (see Figure 2.6). R_0 equals $(\sigma/\bar{T})^2$, the square of the coefficient of variation of the distribution:

$$R_0 = \frac{1}{(\bar{T})^2(N-1)} \sum_{j=0}^{N-1} (T_j - \bar{T})^2 = (\sigma/\bar{T})^2 \tag{2.3}$$

During normal sinus rhythm, the R_i considered as a function of i, are of the form of a damped sinusoid (see Figure 2.6a). Notice that the RR intervals are correlated over delays of more than 20 beats, or equivalently delays of more than 25 seconds. This correlation over long delays reflects the relatively long periodicities associated with physiologic feedback loops involved in heart rate control. Indeed, the detailed shape of the autocovariance function (or its Fourier transform, the power spectrum) contains specific information on both the characteristics of the perturbations to the cardiovascular system, and the dynamics of the feedback loops involved in the compensatory heart rate response [1].

Now consider the autocovariance coefficients during atrial fibrillation. In Figure 2.6b we see that although R_0 is much larger (indicating a larger value of $(\sigma/\bar{T})^2$) during atrial fibrillation than during normal sinus rhythm, the correlation between beats is at least an order of magnitude smaller than R_0 for all delays i greater than or equal to two. The autocovariance coefficient R_1 is

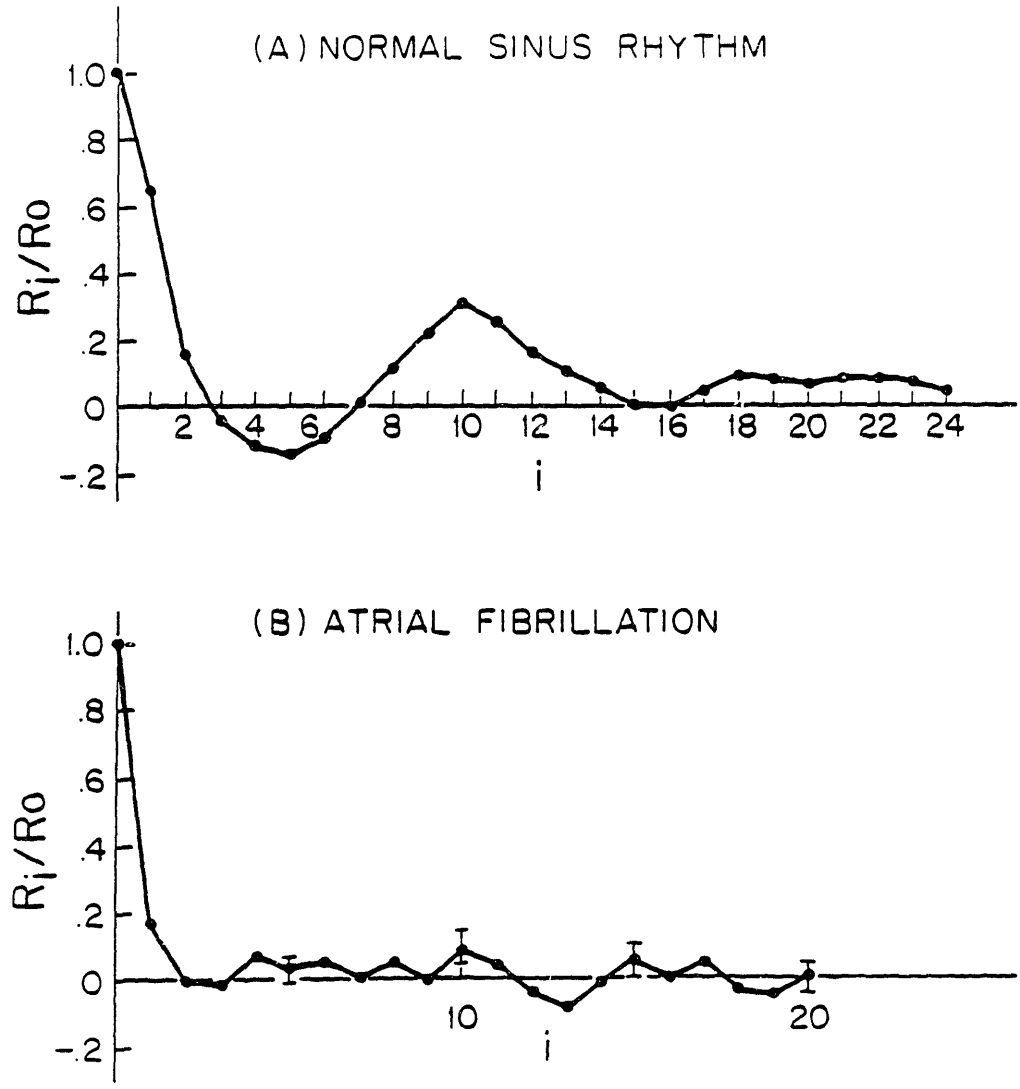

Figure 2.6: Plots of serial autocovariance coefficients of RR interval sequences during normal sinus rhythm (A) and atrial fibrillation (B) in man. In (A), $R_0 = 6.1\times10^{-3}$ and in (B), $R_0 = 3.4\times10^{-2}$. Note that during normal sinus rhythm, RR intervals separated by more than twenty beats are still well correlated. Note that during atrial fibrillation R_0 is much greater than during normal sinus rhythm, indicating a greater absolute variability. During atrial fibrillation, R_1 is significant, but the R_i for $i \geq 2$ do not significantly differ from zero.

significantly greater than zero, but much smaller than R_0 in magnitude. Thus, the RR intervals during atrial fibrillation are essentially statistically independent of each other, except for a slight correlation between the duration of immediately subsequent beats [3,4]. Hoff and Geddes [6,7] have shown that under conditions of high vagal tone, even during atrial fibrillation, the R_i (for $i \geq 2$) may be significantly different from zero; in this case the pattern of variation of R_i with i is similar to that observed during normmal sinus rhythm, but the amplitude of this pattern is reduced compared to the magnitude of R_0. This would suggest that whereas the RR interval variation intrinsic to atrial fibrillation is essentially uncorrelated (except for immediately subsequent beats), strong extrinsic autonomic modulation may impose some degree of correlation.

§2.3 Summary of Statistical Properties of RR Interval Sequence During NSR and Atrial Fibrillation

In summary, during normal sinus rhythm the RR interval statistics are typically characterized by:

(1) a relatively narrow, unimodal RR interval histogram often of a Gaussian form;

(2) autocovariance coefficients R_i which are statistically significant even for large values of i.

The RR interval variation resulting from atrial fibrillation, on the other hand, is characterized by:

(1) an RR interval histogram which may be of a variety of forms varying from a smooth unimodal distribution to a distribution characterized by a smooth background upon which is superimposed a set of evenly spaced narrow peaks;

(2) autocovariance coefficients of which only R_1 is significant compared to R_0.

A high degree of autonomic tone may alter some of these features, leading to non-zero autocovariance coefficients during atrial fibrillation, and making the histogram during normal sinus rhythm non-Gaussian.

Chapter 3

Qunatitative Model for Atrial Fibrillation

In this chapter a simple quantitative model for the genesis of RR interval fluctuations during atrial fibrillation based upon simple electrophysiological concepts is presented. In section 3.1, the model is shown in its simplest form and in the following section a number of modifications are considered.

§3.1 Simplified Model

The motivation of the model begins with the assumption that the turbulent electrical activity in the atria leads to the bombardment of the atrioventricular junction (AVJ) with a series of electrical impulses whach arrive randomly in time at a mean rate λ. (A similar assumption has been made by several other investigators [4,5,8,15]). The arrival of the atrial impulses may be mathematically characterized as a Poisson process.

In order to understand the relationship between the train of randomly arriving impulses and the variability in RR interval, we must quantify the behavior of the AVJ. The overall behavior of the AVJ represents the temporal and spatial summation of the electrical activity of all the cells in this complex structure; no attempt at a detailed microscopic examination of the interactions of these cells is made here. Rather, the model relies upon the empirical clinical observation that a useful characterization of AVJ function can be made in terms of an equivalent single cell description. The atrioventricular junction equivalent cell (AVJEC) is a hypothetical electrically active cell with defined electrical properties (refractory period, automaticity, etc.). The electrical behavior of this hypothetical structure need not correspond to the electrical activity of any real biologic cell located in the AVJ. Indeed, the AVJEC concept is merely a convenient device to understand the input/output characteristics of the AVJ.

In Figure 3.1 the transmembrane potential of the hypothetical AVJEC is shown.

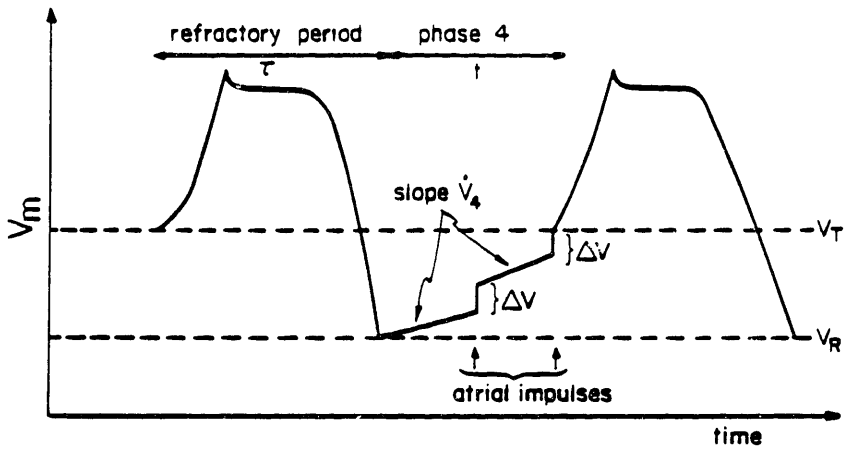

Figure 3.1: Transmembrane potential of hypothetical atrioventricular junction equivalent cell (AVJEC). The action potential, of duration τ, marks the period during which the AVJEC is refractory and is followed by phase four. During phase four the AVJEC depolarizes spontaneously at a rate $\dot{V}_4$, and responds to the arrival of each atrial impulse by depolarizing in a step-wise fashion by an amount ΔV. When the threshold voltage V_T is reached, a new action potential is initiated.

The action potential proper (phases 0, 1, 2, and 3) is of duration τ, during which time the AVJEC is absolutely refractory to stimulation by atrial impulses. The action potential proper is followed by phase four. At the beginning of phase four the transmembrane potential is at its resting value V_R. During phase four the transmembrane potential increases spontaneously at a constant rate $\dot{V}_4$. Each time an atrial impulse arrives during phase four, the transmembrane potential increases by a discrete amount ΔV. When the transmembrane potential reaches its threshold value, V_T, as a result of any combination of stepwise depolarizations and spontaneous phase four depolarization, then the AVJEC fires, initiating a new action potential. (Zipes *et al* [19] present experimental evi-

dence for the summation of impulses in the AVJ as proposed here.)

For the purposes of this model, the AVJ is considered to include not only the AV node itself (AN, N, and NH regions), but also the automatic tissue of the prenodal atrium and proximal Bundle of His. It is important to recognize that the AVJEC is a hypothetical lumped structure used to represent the overall behavior of all these interacting regions of the AVJ. Different attributes of the AVJEC may reflect spatially and temporally dispersed properties of the AVJ. For example, impulse summation may occur in one region, automaticity of the AVJEC may reflect primarily the activity of another region, and the refractory period of the AVJEC might reflect the properties of still another region.

Therefore, one must be careful to interpret the model parameters in terms of the overall functioning of the AVJ. Thus, while the influence of an atrial impulse on a given biological cell may be quite different from the sustained stepwise depolarization depicted for the AVJEC, this may be an accurate way of representing the overall response of the AVJ to an atrial impulse. Furthermore, the amplitude of ΔV reflects not only the activity of individual cells, but also the spatial coherence of this activity. During normal sinus rhythm a synchronous depolarization wavefront arrives at the AVJ and hence ΔV would normally exceed $V_T - V_R$ in amplitude, permitting one-to-one atrioventricular conduction. During atrial fibrillation, loss of spatial coherence in atrial depolarization leads to a decrease in the magnitude of ΔV. As the degree of spatial disorganization increases one would expect ΔV to further decrease; concomitantly, λ would increase as greater depolarization wavefront fractionation leads to the development of many parallel inputs to the AVJ. Finally, τ represents the effective refractory period of the AVJ structure and need not correspond to the refractory period of any individual cell in the AVJ.

One property of the AVJEC not explicitly displayed in Figure 3.1 is the finite time required for impulses to propogate through the AVJ. This delay is, of course, an important property of the AVJEC. However, a fixed or randomly variable conduction delay for atrial impulses will not affect the predicted RR interval distribution during atrial fibrillation because the atrial impulses themselves arrive at the AVJ randomly in time. Therefore, we need not explicitly consider this conduc-

tion delay in analyzing the predictions of the model for atrial fibrillation. However, one would need to explicitly consider the AVJ conduction delay if one were to use the AVJEC concept in analyzing other dysrhythmias.

The simplest form of this model is thus fully characterized by four parameters:

(1) λ - the mean rate at which atrial impulses bombard the AVJEC

(2) $\Delta V/(V_T - V_R)$ - the relative amplitude of the atrial impulses

(3) $\dot{V}_4/(V_T - V_R)$ - the relative rate of phase four depolarization of the AVJEC

(4) τ - the refractory period of the AVJEC.

The statistics of the RR interval sequence predicted by this model in its simplest form can now be analyzed. First, we note that the model predicts that there will be no correlation between the duration of different RR intervals since the RR interval variation is being driven by a Poisson process which has no memmory. Next we consider the predicted RR interval histogram. The refractory period of the AVJEC is assumed here to be constant from one beat to the next. The magnitude of the refractory period affects the histogram only by shifting it to the right on the time axis by an amount τ, since no RR interval can be shorter than the refractory period. The structure of the histogram beyond the refractory period may be considered in three cases. (For detailed mathematical analysis see Appendix A.)

First, we consider the appearance of the RR interval histogram when the depolarization of the AVJEC during phase four is dominated by the arrival of atrial impulses, and spontaneous phase four depolarization is, by comparison, negligible. Expressed mathematically, this occurs when

$$\frac{\lambda \Delta V}{V_T - V_R} >> \frac{\dot{V}_4}{V_T - V_R} \tag{3.1}$$

In this case the transmembrane potential will reach the threshold level only after $(V_T - V_R)/\Delta V$ atrial impulses have arrived at the AVJ since the beginning of phase four. (Note that if $(V_T - V_R)/\Delta V$ is not an integer, then the number of impulses required to reach the threshold is the next higher integer.) The resulting histogram will be described by an Erlang curve shifted to the right by an amount equal to the refractory period. In this special case, this model becomes very

similar to that of Hashida *et al* [5]. As these investigators noted, Erlangian histograms are marked by a single broad peak (see Figure 2.2b).

The case just considered corresponds to the situation where ventricular excitation is controlled by an atrially dominated process, and the spontaneous automaticity of the AVJ contributes to a negligible extent. A second special case corresponds to the opposite extreme, in which the rise in the transmembrane potential during phase four is dominated by the spontaneous rate of phase four depolarization, and the arrival of atrial impulses contributes to a negligible degree. In this case,

$$\frac{\lambda \Delta V}{V_T - V_R} << \frac{\dot{V}_4}{V_T - V_R} \tag{3.2}$$

Ignoring atrial activity altogether, we see that a new action potential will be triggered once the transmembrane potential of the equivalent cell has ramped up to the threshold level as the result of the spontaneous depolarization caused by automatic tissue within the AVJ region. Theoretically, we would predict a duration of $\tau + (V_T - V_R)/\dot{V}_4$ for every RR interval when this special case applies. The resulting histogram will obviously be a single very narrow peak. This special case corresponds to the limit of junctional tachycardia often seen in atrial fibrillation patients, particularly in the situation of digitalis toxicity.

Finally, we consider the third situation when both the arrival of atrial impulses and the spontaneous depolarization contribute significantly to the increase in the transmembrane potential during phase four. This is the most interesting situation because the resulting RR interval histogram combines features from those seen in both extreme cases. The histogram now includes several narrow peaks superimposed at regular intervals on a background composed of sections of Erlang curves as seen in Figure 2.4b. A mathematical derivation of this surprising result appears in Appendix A. One may understand the form of the distribution qualitatively by considering Figure 3.2 in which the behavior of the transmembrane potential of the AVJEC during phase four is depicted. One sees that there are two possible ways for V_m to finally reach the threshold value V_T: (A) it can slide up to V_T as a result of the spontaneous phase four depolarization, or (B) it can jump over V_T as the result of the arrival of an atrial impulse. In Case A, the times at which V_T is reached are

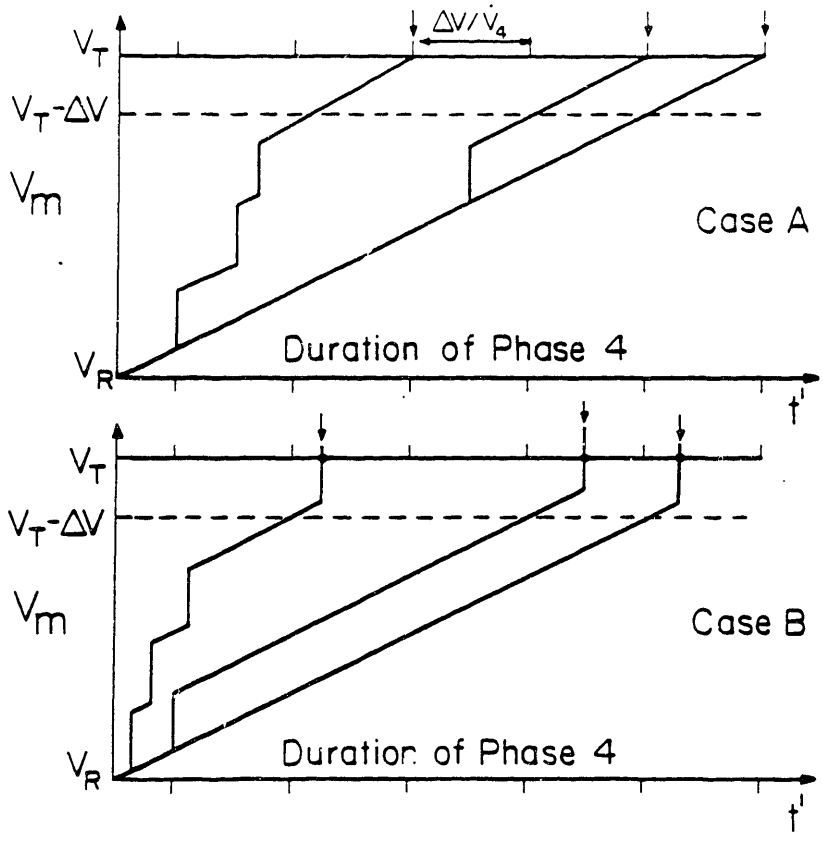

Figure 3.2: Possible time course of transmembrane potential of AVJEC during phase four. In Case A the final mechanism by which V_m reaches threshold is the spontaneous phase four depolarization. In Case B the final event to bring V_m past threshold is the arrival of an atrial impulse.

quantized and given by

$$T = \tau + \frac{V_T - V_R - n\Delta V}{\dot{V}_4}$$

$$= \tau + \frac{1 - n\left[\frac{\Delta V}{V_T - V_R}\right]}{\left[\frac{\dot{V}_4}{V_T - V_R}\right]} \qquad (3.3)$$

In Case A the duration of the RR interval T is determined only by n, the number of impulses that arrived during phase four, and not by the precise times of their arrival. Case A corresponds to the set of discrete evenly spaced peaks in the histogram. In Case B, on the other hand, the final event to bring the transmembrane potential over threshold is the arrival of an atrial impulse. Since atrial impulses have a constant probability per unit time of arrival, Case B will correspond to the smooth portions of the histogram. Thus, this very simple model can account for a wide variety of possible nistogram structures. The model directly predicts the multiple peaked histograms predicted by Söderström [16] and other investigators. The single-peaked and the bimodal histograms seen by Horan and Kistler [10] and by Goldstein and Barnett [4] also conform to possible results predicted by the model, given the correct choice of the four parameters in each case.

§3.2 Modified Model

A number of minor modifications to the model just presented will now be considered. The initial version of the model correctly predicts the general forms of the RR interval histogram during atrial fibrillation, and also predicts that the RR intervals will be uncorrelated with each other. However, as noted in section 2.2, the first autocovariance coefficient R_1 is experimentally found to be positive indicating a positive correlation between immediately subsequent intervals. In fact, one could expect this correlation since the refractory period of a cell depends on the duration of the preceding interbeat interval [14]. The model can thus be modified to indicate that the refractory period, τ, of the AVJEC is not fixed but depends on the preceding RR interval. This relationship may be parameterized using the data of Mendez *et al* [14] as follows:

$$\tau_i = \tau_\infty \left[1 - e^{-T_{i-1}/\tau_\infty}\right] \tag{3.4}$$

This relationship is plotted in Figure 3.3. It is readily apparent that the refractory period of the i^{th} beat, τ_i, is a monotonically increasing function of T_{i-1}, the duration of the preceding RR interval. When T_{i-1} is much smaller than τ_∞, then τ_i varies linearly with T_{i-1}. When T_{i-1} is much greater than τ_∞, τ_i approaches its maximum value of τ_∞. Notice that this modification of the original model does not alter the number of adjustable parameters. τ_∞ just replaces τ as the fundamental parameter.

It must be emphasized that the dependence of τ_i on T_{i-1} described by equation 3.4 represents the integrated behavior of the entire AVJ. Individual cells within the AVJ may have refractory periods which depend on the interbeat interval in quite a different way. For the purposes of this model and for the measurements of Mendez *et al* [14], it is the overall behavior of the AVJ that is relevant.

The initial version of the model predicts that the evenly spaced peaks in the RR interval histogram are arbitrarily narrow. This of course, is unrealistic. A finite peak width would result if one assumed that the quantum depolarization, ΔV, is not fixed at a single value, but may vary somewhat about a mean. Similarly, slight beat-to-beat variations in τ (or τ_∞) or in $\dot{V}_4/(V_T - V_R)$ would result in the broadening of these peaks. (Fluctuations in τ_i depending solely on T_{i-1} can be

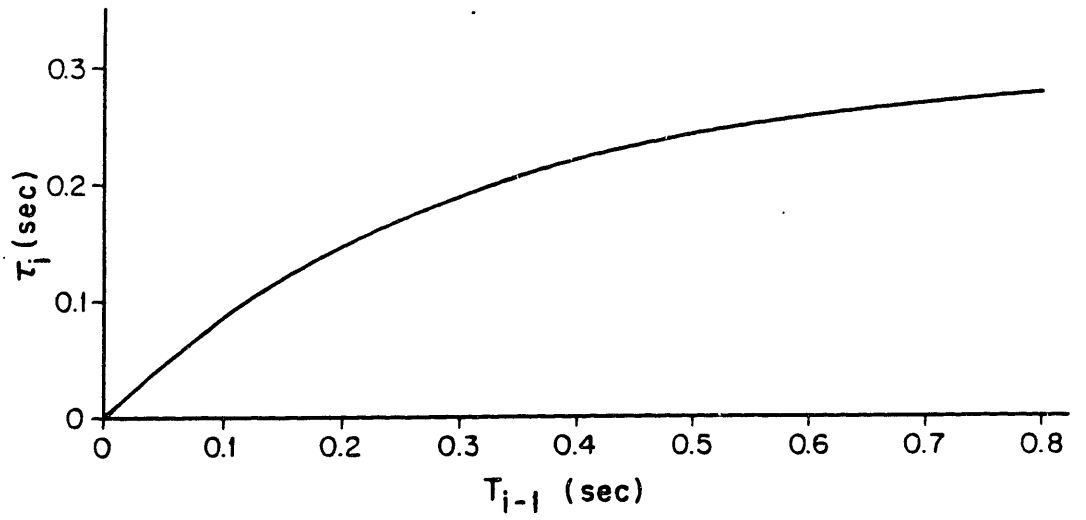

Figure 3.3: Graph of the relationship $\tau_i = \tau_\infty \left[1 - e^{-T_{i-1}/\tau_\infty}\right]$ used to correct for the correlation between immediately consecutive RR intervals. In this example, $\tau_\infty = 0.3$ sec. The plot is extrapolated to $T_{i-1} = 0$ although obviously no experimental points lie near $T_{i-1} = 0$. The data correction procedure is described in section 4.4.

removed by use of equation 3.4. This discussion refers to broadening of the peaks which persists after such correction is performed.) It is not necessary, however, to make any specific assumptions regarding such slight variations in the model's parameters. Furthermore, under conditions of high levels of autonomic modulation, one might consider each of the model's parameters to be modulated by autonomic activity. This would lead to some 'smearing' of the histogram, and the imposition of non-zero autocorrelation coefficients as noted by Hoff and Geddes [6,7].

Thus, the original version of the model is modified to explicitly take into account the dependence of the refractory period on the duration of the preceding RR interval. This modified version of the model predicts the correct form of the RR interval histogram, as well as the autocovariance

coefficients, which differ significantly from zero for $i \leq 1$. Furthermore, it is not inconsistent with the model that slight physiologic beat-to-beat variation in the model parameters makes the peaks in the histogram be of finite width, and that strong autonomic modulation of the parameters will further smear the histogram and may force the autocovariance coefficients, R_i to be non-zero even when i is greater than unity. Thus, the intrinsic variability of the RR interval during atrial fibrillation is essentially uncorrelated, but strong extrinsic autonomic modulation may superimpose some degree of long-term correlation.

One interesting situation may occur as a result of the 'blurring' of the histogram from slight physiologic variation in the model's parameters. Consider the case where the spacing between the peaks in the histogram, $\Delta V / \dot{V}_4$ (see equation 3.3), is very small. In this case, slight smearing of these peaks may lead to an apparently unimodal distribution, even though a large number of evenly spaced peaks are actually present. Such a case in which the separate peaks in the experimental distribution are just at the limits of resolution is shown in Figure 2.5.

Finally, it is important to recognize that the model presented here need not explicitly deal with the finite delay associated with transmission through the AVJ. This delay would not affect the RR interval distribution provided that the delay is of constant or randomly varying magnitude.

Chapter 4

Experimental Methods

§4.1 Surgical Preparation of Dog Model

In order to test the validity of this AVJEC model for atrial fibrillation, the RR interval statistics predicted by this model were compared with those computed from RR interval sequences recorded from dogs in which atrial fibrillation was electrically induced. Surgical implantation of epicardial stimulating electrodes was performed on adult dogs following a procedure similar to that of Whittington *et al* [18]. After anesthesia was induced with sodium pentabarbital, the chest was opened using full aseptic technique via the fourth right intercostal space. Two electrodes were sutured to the right atrial appendage and mid-right atrial wall for electrical stimulation of the right atrium, and two other electrodes were sewn to the right ventricular wall to allow for a cardiac electrogram signal. The wires were exteriorized via small stab incisions 3 cm caudal to the chest incision. In addition, catheters were placed in the right femoral artery and vein using a purse string stitch in each vessel wall, thereby maintaining patency of the vessels distal to the point of catheter placement. The catheters were taken via subcutaneous tunnels and exteriorized through small stab incisions made near those for the epicardial electrodes. These provided a convenient route for intravenous infusion of drugs and a means for monitoring arterial blood pressure.

§ 4.2 AC Current Source for Electrical Induction of Atrial Fibrillation

Electrical stimulation of the atria of the canine heart with 60Hz alternating current induces a cardiac arrhythmia that is electrocardiographically indistinguishable from atrial fibrillation [18]. An AC current source was designed and built to provide 60Hz current adjustable from 0 to 100 milliamperes RMS. A schematic drawing of the electronic circuitry of this current source is shown in figure 4.1.

While electrical stimulation of the atria does reproducibly induce the fibrillatory state, it unfortunately also adds a 60Hz artifact in the cardiac electrogram signal measured between the two ventricular epicardial electrodes. This artifact was easily filtered out using a 50db deep 60Hz notch filter of the design shown in Figure 4.2.

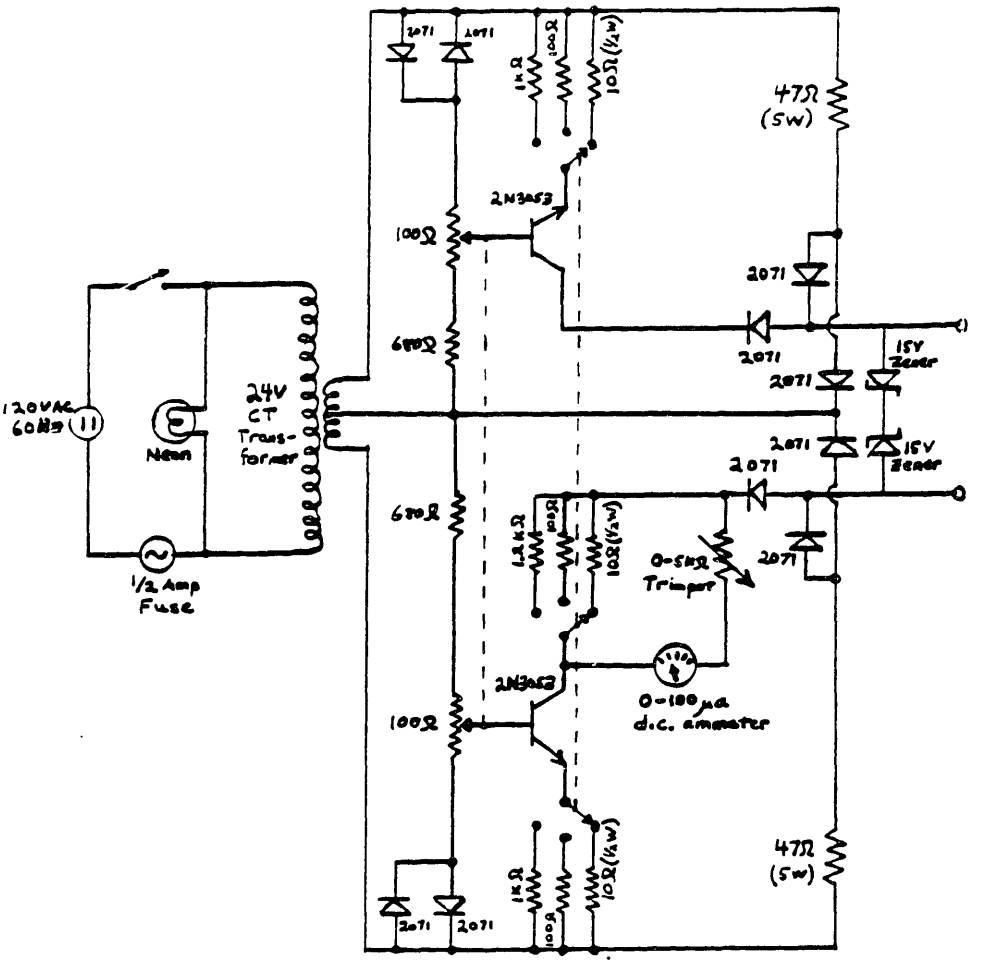

Figure 4.1: Schematic of the AC current source used for electrical induction of atrial fibrillation in dogs. The output current can be adjusted from 0.1ma to 100ma RMS in three decade ranges.

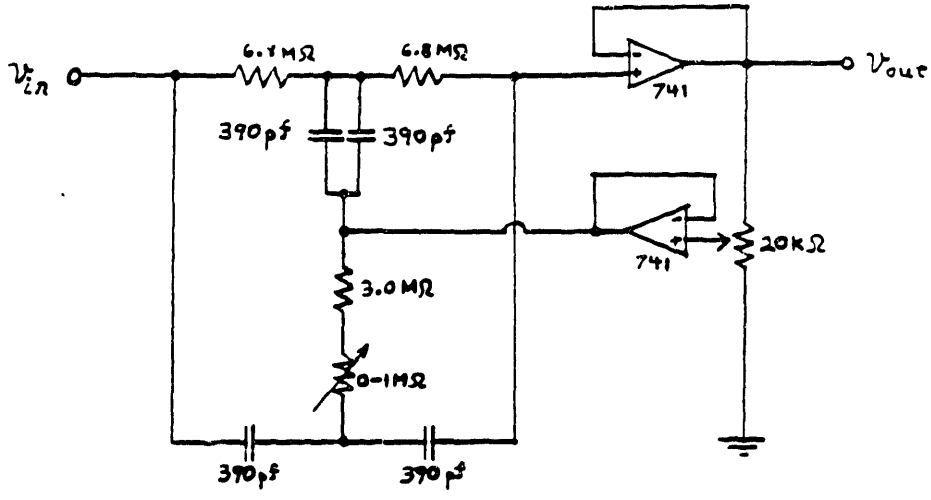

Figure 4.2: Schematic of 60Hz notch filter providing 50db rejection of the 60Hz artifact in the cardiac electrogram caused by electrical induction of atrial fibrillation.

§4.3 Protocol of Dog Experiments

Induction of atrial fibrillation by electrical stimulation was performed on dogs instrumented with epicardial electrodes as described in section 4.1. Although many experiments were attempted in which atrial fibrillation was induced in fully conscious dogs, wide fluctuations in the dogs' state of arousal from minute to minute, and hence changes in sympathetic and parasympathetic tone, rendered most of the data from these experiments too nonstationary for analysis. Therefore, all experiments discussed in this thesis were performed on dogs anesthetized with sodium pentabarbital administered by either periodic bolus injections or continuous infusion.

After induction of anesthesia, a cardiac electrogram signal from the ventricular epicardial electrodes was monitored and continuously recorded on a Hewlett Packard model 3968A eight track tape recorder. The AC current source described in section 4.2 was connected to the atrial epicardial electrodes, and atrial fibrillation was induced. While 1ma was generally sufficient for induction of atrial fibrillation, all experiments were performed using a stimulating current of 4ma RMS. The stimulation artifact was filtered out of the cardiac electrogram using the 60Hz filter described in section 4.2.

Several different pharmacologic agents frequently employed in the clinical management of atrial fibrillation were tested in terms of their effects on the values of the four model parameters. Such agents included a digitalis glycoside (ouabain), a β-adrenergic blocker (propranolol), and the anti-arrhythmic agents procaine amide, quinidine, and verapamil. The results of an exemplary digitalis experiment are included in this thesis. (See section 5.2.) The drug being tested in any given experiment was infused using a Harvard Apparatus infusion pump via the femoral vein catheter. The infusion rate was either maintained constant or increased at regular intervals throughout the experiment to achieve increasing blood levels of the drug. Digitalis infusions were terminated when signs of toxicity such as consecutive premature ventricular beats occurred.

The recorded cardiac electrogram signals were analyzed later using the algorithm described in the following section.

§4.4 Algorithm for Analysis of Experimental Data

In order to deduce from an experimentally obtained sequence of RR intervals the numerical magnitudes of the four model parameters that best fit the experimental data, an algorithm was developed for implementation on a Digital Equipment Corporation MINC-11 computer. The cardiac electrogram signals recorded in the animal experiments described in the previous section were played back at real-time speed and sampled at 1kHz. RR intervals were measured as the time difference between peaks of successive R waves. Files of 1000 consecutive RR intervals were then analyzed with the BASIC program shown in Appendix C.

1000 consecutive RR intervals is sufficient to deduce statistically significant values for the four model parameters, yet generally represents a sufficiently short time period of data collection so as to be free of trend-like variations in the parameter values with time. Occasionally, however, an increasing or decreasing trend in RR interval duration will occur over the 5 to 10 minutes required to acquire 1000 RR intervals. This trend, superimposed on the intrinsic variability of the fibrillating heart system, is presumably caused either by the slowly increasing blood levels of the drug being tested or by fluctuations in the depth of anesthesia. In order to compensate for such trends, the analysis algorithm first adjusts each RR interval so as to produce a trendless sequence of RR intervals that preserves the intrinsic variability. This is accomplished by fitting a line to a plot of RR interval duration *vs* time using linear regression, and then subtracting from each RR interval the amount of time corresponding to the difference between this fitted line and a line of zero slope whose y-intercept is equal to the mean RR interval duration.

After having corrected for linear trends, it is still necessary to compensate for the dependence of the refractory period on the duration of the previous RR interval as discussed in section 3.2. A binary search is employed to locate the value of τ_∞ that minimizes the variance of $(T_i - \tau_i)$ where T_i is the duration of the i^{th} RR interval in the sequence and

$$\tau_i = \tau_\infty \left[1 - e^{T_{i-1}/\tau_\infty}\right] \tag{4.1}$$

Once τ_∞ is determined, each RR interval is adjusted so that

$$T_{i_{new}} = T_{i_{old}} - \tau_i + \bar{\tau} \tag{4.2}$$

where $\bar{\tau}$ is the mean of all τ_i. The procedure described here for correcting the RR interval data is only weakly dependent on the actual form of equation 4.1, and in essence corresponds to an inverse filtering procedure for eliminating correlation between subsequent intervals.

The corrected sequence of RR intervals is then passed to the next process in the computer program, which deduces optimal values for the model parameters λ, τ, N, and ν, where

$$N = \frac{V_T - V_R}{\Delta V}$$

$$\nu = \frac{\dot{V}_4}{\Delta V}$$

The basic approach used to deduce these parameters is to (1) try a set of values for λ, τ, N, and ν; (2) calculate the 'theoretical' RR interval histogram predicted by the model for these parameter values; (3) evaluate the 'goodness of fit' between this theoretical histogram and the experimental histogram; and (4) try a new set of values for λ, τ, N, and ν, and repeat the process until the theoretical histogram fits the experimental histogram as closely as possible.

In order to evaluate the goodness of fit between the theoretical and experimental histograms, an error function is defined which measures the area between the corresponding cumulative probability curves $P_t(T)$ and $P_e(T)$. $P_t(T)$ is defined as the fraction of RR intervals in the theoretical distribution whose duration is shorter than T. $P_e(T)$ is defined similarly for the experimental distribution. The error function is thus:

$$E = \frac{\int_0^\infty \left[\left\{P_t(T) - P_e(T)\right\}^2\right]^{1/4} dT}{\int_0^\infty \left[P_e(T)\left\{1 - P_e(T)\right\}/M\right]^{1/4} dT} \tag{4.3}$$

where M is the number of RR intervals in the experimental sequence. This error function is normalized so that its expectation value is unity when all systematic differences between experimental and theoretical distributions are eliminated, and the only differences between the two distributions that remain are those attributable to the statistical uncertainty in the experimental data anticipated from the use of a finite number of RR intervals.

As is further discussed in Appendix A, a set of λ and τ uniquely determines a family of Erlang curves. N and ν uniquely determine a set of evenly spaced delta-functions at which the theoretical RR interval histogram jumps from one Erlang curve to the next. The search algorithm employed to find the four parameter values that minimize the error function is as follows:

(1) A range over which to search for τ is defined as $0 < \tau < T_{.005}$, where $T_{.005}$ is the time such that exactly 0.5% of all RR intervals in the sequence are shorter than it. A 'golden section' search over this range for τ is performed; bookkeeping variables are defined as:

$$x_1 = 0$$
$$x_4 = T_{.005}$$
$$x_2 = .618x_1 + .382x_4$$
$$x_3 = .382x_1 + .618x_4$$

Steps (2) through (5) are then performed for $\tau = x_2$, and then for $\tau = x_3$.

(2) For a given value of τ, a range over which to search for λ is defined as $0 < \lambda < (<T> - \tau)/\mu_2$, where $<T>$ is the mean RR interval duration and μ_2 is the variance of the RR intervals. As is done for τ, a golden section search for λ is performed over this range, and again bookkeeping variables are defined:

$$y_1 = 0$$
$$y_4 = (<T> - \tau)/\mu_2$$
$$y_2 = .618y_1 + .382y_4$$
$$y_3 = .382y_1 + .618y_4$$

Steps (3) and (4) are then performed for $\lambda = y_2$, and then for $\lambda = y_3$.

(3) Given a set of values for τ and λ, the family of Erlang curves specified by these two parameters is

$$p_i(T) = \frac{\lambda^{i+1} e^{-\lambda(T-\tau)}(T-\tau)^i}{i!} \tag{4.4}$$

These curves can each be integrated to generate a family of 'integrated Erlang curves,'

$$P_i(T) = 1 - \sum_{k=0}^{i} e^{-\lambda(T-\tau)}\lambda^k (T-\tau)^k / k! \tag{4.5}$$

A new family of curves can then be defined as those curves that run equidistantly between two adjacent integrated Erlang curves:

$$\tilde{P}_i(T) = 1 - \left[\sum_{k=0}^{i-1} e^{-\lambda(T-\tau)}\lambda^k(T-\tau)^k/k! + \frac{e^{-\lambda(T-\tau)}\lambda^i(T-\tau)^i}{2i!}\right] \quad (4.6)$$

The points where this family of curves, $\tilde{P}_i(T)$, intersect the experimental cumulative probability curve, $P_e(T)$, are the optimal locations for the delta-functions at which the theoretical distribution jumps between Erlang curves. Only those points of intersection that occur between $.01 < P_e(T) < .99$ are taken as statistically significant. While a set of N and ν uniquely determines the set of these intersection points, a set of intersection points uniquely determines N and ν only if there are two or more such points. If there are no such intersection points, N and ν can not be determined uniquely, but ranges of allowed values on each of these parameters are determined. In this case, the theoretical distribution best fits the experimental histogram by following a single one of the Erlang curves within the family specified by τ and λ. If there is one intersection point between the family of curves $\tilde{P}_i(T)$ and $P_e(T)$, then again ranges of values are determined for N and ν. The resulting theoretical distribution in this case will involve pieces from two Erlang curves within the family. If there are exactly two intersection points, then N and ν are determined explicitly as

$$\nu = \frac{1}{T_2 - T_1} \quad (4.7a)$$

$$N = i_1 + \nu T_1 \quad (4.7b)$$

where T_1 and T_2 are the times of the two intersection points that satisfy

$$\tilde{P}_{i_1}(T_1) = P_e(T_1)$$

and

$$\tilde{P}_{i_2}(T_2) = P_e(T_2)$$

If there are more than two such intersection points, then N and $-\nu$ are determined by the y-intercept and slope respectively of a line which best fits the points (i_1,T_1), (i_2,T_2), ..., (i_n,T_n) on a plot of i vs T where each pair, i_k and T_k, satisfy

$$\tilde{P}_{i_k}(T_k) = P_e(T_k)$$

(4) Once the optimal theoretical distribution for a given choice of τ and λ has been specified [in step (3)], then the error function is calculated.

(5) E_2 and E_3 are defined as the values of the error function at $\lambda = y_2$ and $\lambda = y_3$ respectively. The golden section search for λ is then moved one step further as follows:

if $E_2 \leq E_3$, then set

$$y_{1_{new}} = y_{1_{old}}$$
$$y_{3_{new}} = y_{2_{old}}$$
$$y_{4_{new}} = y_{3_{old}}$$
$$y_{2_{new}} = .618\, y_{1_{new}} + .382\, y_{4_{new}}$$
$$E_{3_{new}} = E_{2_{old}}$$

Then set $\lambda = y_{2_{new}}$ and go back to step (3).

if $E_3 < E_2$, then set

$$y_{1_{new}} = y_{2_{old}}$$
$$y_{2_{new}} = y_{3_{old}}$$
$$y_{4_{new}} = y_{4_{old}}$$
$$y_{3_{new}} = .382\, y_{1_{new}} + .618\, y_{4_{new}}$$
$$E_{2_{new}} = E_{3_{old}}$$

Then set $\lambda = y_{3_{new}}$ and go back to step (3).

For a given value of τ, steps (3) through (5) are repeated for a total of six iterations.

(6) F_2 and F_3 are defined as the values of the error function for the final value of λ at $\tau = x_2$ and $\tau = x_3$ respectively. Using F_2 and F_3 in place of E_2 and E_3 and a procedure for updating x_1, x_2, x_3, and x_4 identical to that used for updating y_1, y_2, y_3, and y_4 in step (5), a golden section search for τ is advanced one step.

Steps (2) through (6) are repeated for a total of eight iterations. The final values for λ, τ, N, and ν as well as the associated minimal value of the error function are then reported, and the corresponding theoretical RR interval distribution is plotted for comparison with the experimental histogram.

Chapter 5

Results

§ 5.1 Comparison of Model with Experimental Data

In Figures 2.2 through 2.5 experimental RR interval histograms obtained from patients in chronic atrial fibrillation, or dogs in which atrial fibrillation was electrically induced as described in section 4.3, are compared with the predictions of the model. The model was fitted in each case using the algorithm described in section 4.4. In general, the model was able to account for both unimodal histograms and histograms with multiple peaks. The parameters λ and τ were reliably determined from most stationary RR interval sequences. However, the parameters $\Delta V/(V_T - V_R)$ and $\dot{V}_4/(V_T - V_R)$ could be determined uniquely only when at least two peaks were present in the histogram, as discussed in section 4.4.

The values of λ obtained by fitting the distributions in Figures 2.2 through 2.5 vary from 5/ sec to 116/ sec. These values of λ should not be construed to represent the actual impulse rate at a single site in the atrium or AVJ, but may rather represent summation of impulses in many cells depending on the degree of spatial disorganization.

The experimental distributions differ from the theoretical distributions primarily in that the experimental peaks are of finite width as opposed to the arbitrarily narrow theoretical delta functions (which are represented as having a width corresponding to one histogram bin in Figures 2.2 through 2.5). Thus, the peaks in the experimental histograms are of lower amplitude and are broader than the taller and narrower peaks representing delta functions in the theoretical histograms. The numerical magnitudes of the fundamental parameters of the model may be determined without explicitly determining the finite widths of the peaks. However, once these parameters are determined, an additional parameter, s, corresponding to the intrinsic width of the peaks could be deduced by representing each theoretical delta function by a Gaussian curve and adjusting the width of the Gaussian to optimize the fit between theoretical and experimental distributions.

§ 5.2 Quantitative Characterization of the Effects of Digitalis

The results of a pharmacologic study in which the dose response of the digitalis glycoside, ouabain, is characterized in terms of changes in the numerical magnitudes of the model's four parameters is presented in Figure 5.1. Bolus injections of .2mg ouabain were administered every half hour over a three hour period (and then tapered to .1mg and finally .05mg injections) following the protocol outlined in section 4.3.

For all but the initial baseline RR interval sequence, only a single peak appeared in the experimental RR interval histogram. Consequently, ranges for $\Delta V/(V_T - V_R)$ and $\dot{V}_4/(V_T - V_R)$ were determined throughout the experiment, but unique values for these parameters could not be. Values for λ and τ, however, were deducible, and trends in these parameters with increasing digitalis dose are easily appreciated. The fall in mean ventricular rate with increasing digitalis dose appears to be almost completely due to a steady decrease in λ, the mean rate of arrival of atrial impulses at the AVJ. The refractory period, τ, remains nearly constant throughout the administration of digitalis, and suggests the lengthening of mean RR interval duration can not be explained by a lengthening of the refractory period of the AVJ.

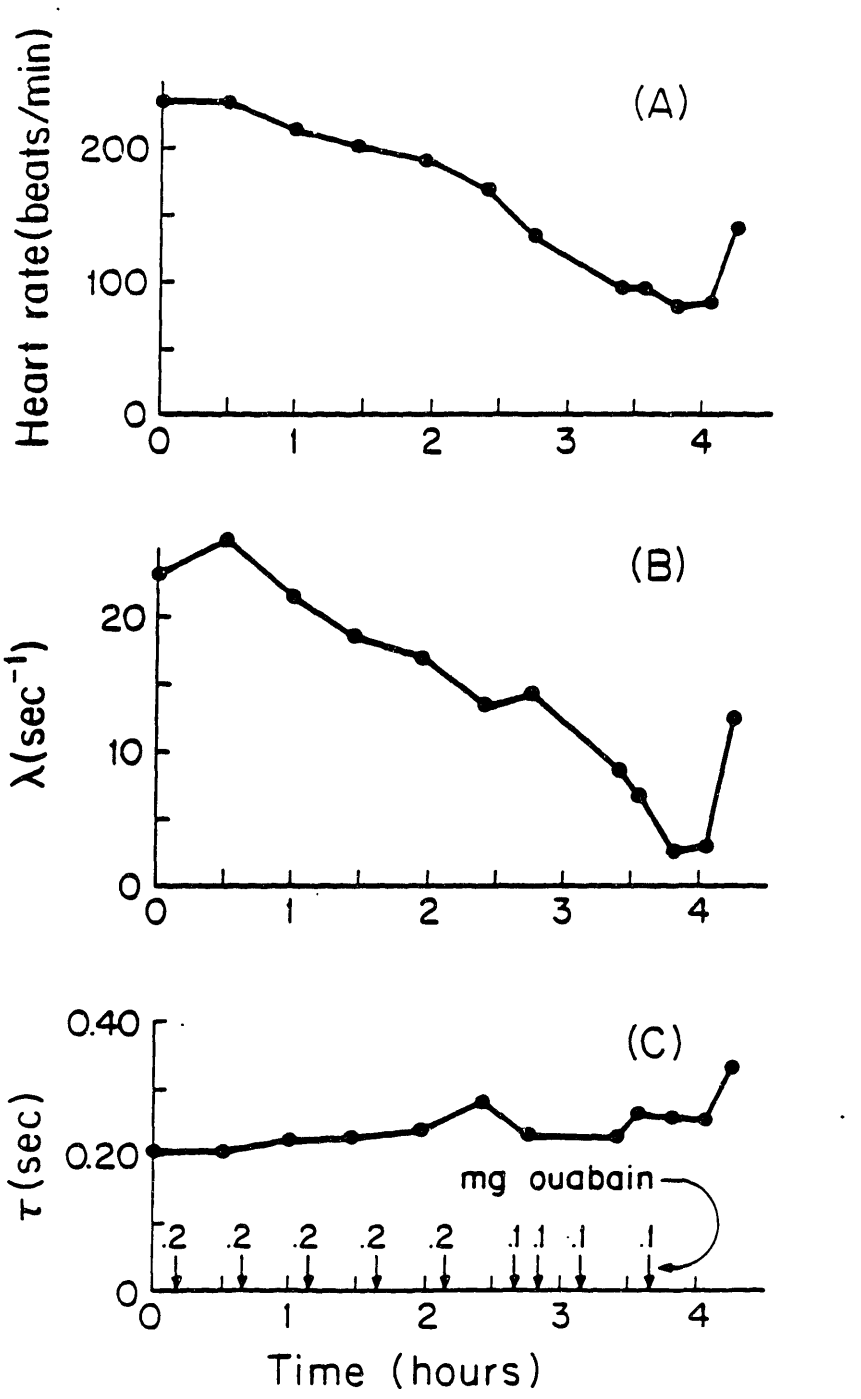

Figure 5.1: Quantitative representation of dose response of dog in atrial fibrillation to the digitalis glycoside ouabain. The heart rate response is shown in (A), and the response of the model parameters λ and τ are shown in (B) and (C) respectively. Ouabain injections are indicated on the time axis.

Chapter 6

Discussion

The model presented here for the genesis of RR interval fluctuations during atrial fibrillation accounts for all the principal statistical features of the RR interval sequence. Furthermore, for a given individual in atrial fibrillation, it is possible to deduce the numerical magnitudes of some or all of the model's four parameters by analysis of 1000 sequential RR intervals. It is most significant that this simple model based on such familiar clinical and electrophysiologic concepts as a refractory period, automaticity, and partial depolarization predicts the unobvious result of multiple narrow peaks in the RR interval histogram.

Previous models of atrial fibrillation require the assumption that the intrinsic behavior of the AVJ during atrial fibrillation differs from that during normal sinus rhythm. For example, the 'concealed conduction' model presented by Moe and Abildskov [15] assumes the AVJ behaves as two separate components with different refractory periods. It is more attractive to assume that the behavior of the atria alone differs between atrial fibrillation and normal sinus rhythm. In terms of the model presented in this thesis, the functioning of the AVJ during normal sinus rhythm could be thought of as identical to that described for atrial fibrillation, but with ΔV greater than or equal to $V_T - V_R$, so that a ventricular activation is initiated in response to every atrial event. Since atrial depolarization is triggered by the sino-atrial (SA) node during normal sinus rhythm, ventricular depolarization will, in turn, be controlled by SA nodal activity. As the SA nodal rate is influenced by autonomic input, the sequence of RR intervals displays the fluctuations characteristic of normal sinus rhythm. Thus, a change in just a single model parameter, $\Delta V / (V_T - V_R)$, instead of a major alteration in overall input/ output behavior of the AVJ, is sufficient when combined with the change in atrial electrical activity to account for the dramatic differences in RR interval statistics seen during atrial fibrillation and normal sinus rhythm. In fact, the model of the AVJ presented here can account for a variety of dysrhythmias associated with a normal pattern of atrial activation, including Mobitz type I and Mobitz type II heart block. These dysrhythmias occur when $\Delta V / (V_T - V_R) < 1$.

It is interesting to analyze the RR interval statistics predicted by previous models of atrial fibrillation. Although the characteristic features seen in the RR interval histogram and autocorrelation function during atrial fibrillation mentioned earlier have all been noted in the literature, none of theories previously presented can account for the wide variety of structures that the histogram may assume. The most widely discussed theory of atrial fibrillation is the concealed conduction concept. The fundamental notion involved here is that an atrial impulse may be totally blocked from entering the AVJ, may enter and propogate part of the way through the AVJ, or may enter and successfully penetrate all of the way through the AVJ and initiate ventricular activation, depending on the levels of refractoriness of the proximal and distal regions of the AVJ (Figure 6.1). Langendorf *et al* [13] first presented this theory, and several models of atrial fibrillation based on the concealed conduction theory or variations thereof have since appeared in the literature.

In the Moe and Abildskov model cited above [15], each of the two regions of the AVJ are assumed to be capable of existing in either of two possible states: refractory or excitable (see Figure 6.1). As in the model presented in this thesis, atrial impulses are assumed to arrive at the top of the AVJ randomly in time. If an atrial impulse arrives at the AVJ when the proximal region is refractory, the atrial impulse is ignored. If, however, the proximal region is in the excitable state, the electrical impulse propogates through to the top of the distal region. If this region is also excitable, the impulse travels completely through the AVJ and initiates ventricular activation, and refractory periods in both regions of the AVJ begin. But if the distal region of the AVJ is refractory upon arrival of the electrical impulse, then propogation ceases, the impulse is 'concealed,' and a new refractory period begins only in the proximal region of the AVJ. The duration of the refractory period of each region is assumed to be a function of the time elapsed since that region was last activated, although the distal region is generally assumed to have a longer intrinsic refractory period than the proximal region. As shown in Appendix B, the Moe and Abildskov model predicts a bimodal histogram. This histogram will approach a unimodal form as the refractory period of the distal region, τ_d, is reduced to the duration of the refractory period of the proximal region, τ_p. Such a histogram is plotted in Figure 6.2. Note that the two peaks are both smooth and broad. Experimental

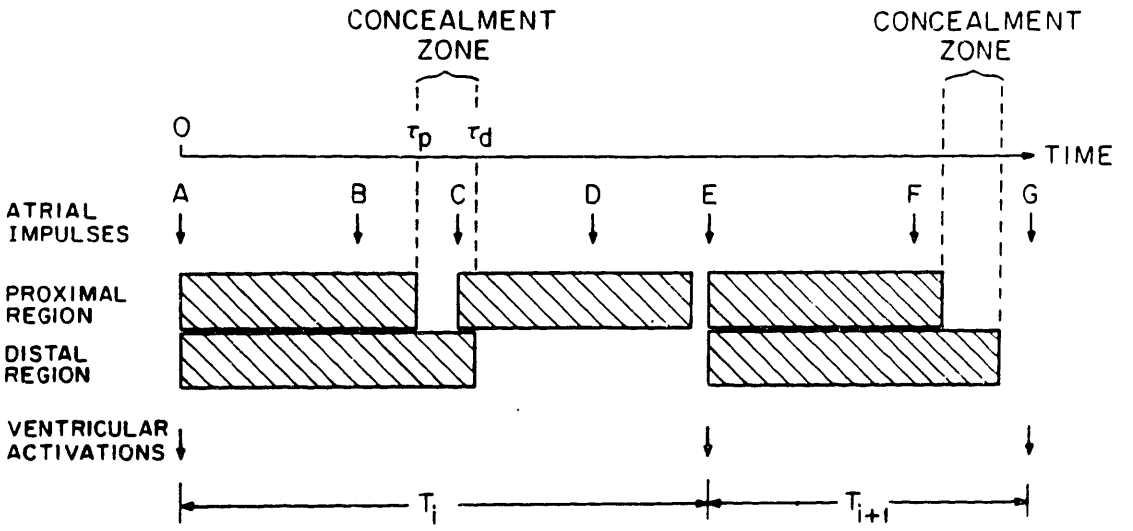

Figure 6.1: Schematic representation of the Moe and Abildskov [15] version of the 'concealed conduction' model for atrial fibrillation, simplified by assuming the refractory periods of the proximal and distal regions of the AVJ, τ_p and τ_d, are constant. Atrial impulse A arrives at the AVJ and propagates through both proximal and distal regions, thus initiating refractory periods in both regions, as well as ventricular activation. This marks the start of RR interval T_i. Impulses B, D, and F are ignored by the AVJ since the proximal region is refractory when each of these impulses arrives. Impulse C arrives during the concealment zone, thus initiating a new refractory period in the proximal region without being able to traverse the distal region. Impulse E arrives when the AVJ is once again excitable and propagates through the entire AVJ to initiate a ventricular activation. This marks the end of RR interval T_i and the beginning of interval T_{i+1}. Inpulse G is the next one to be successfully propogated, and marks the end of RR interval T_{i+1}.

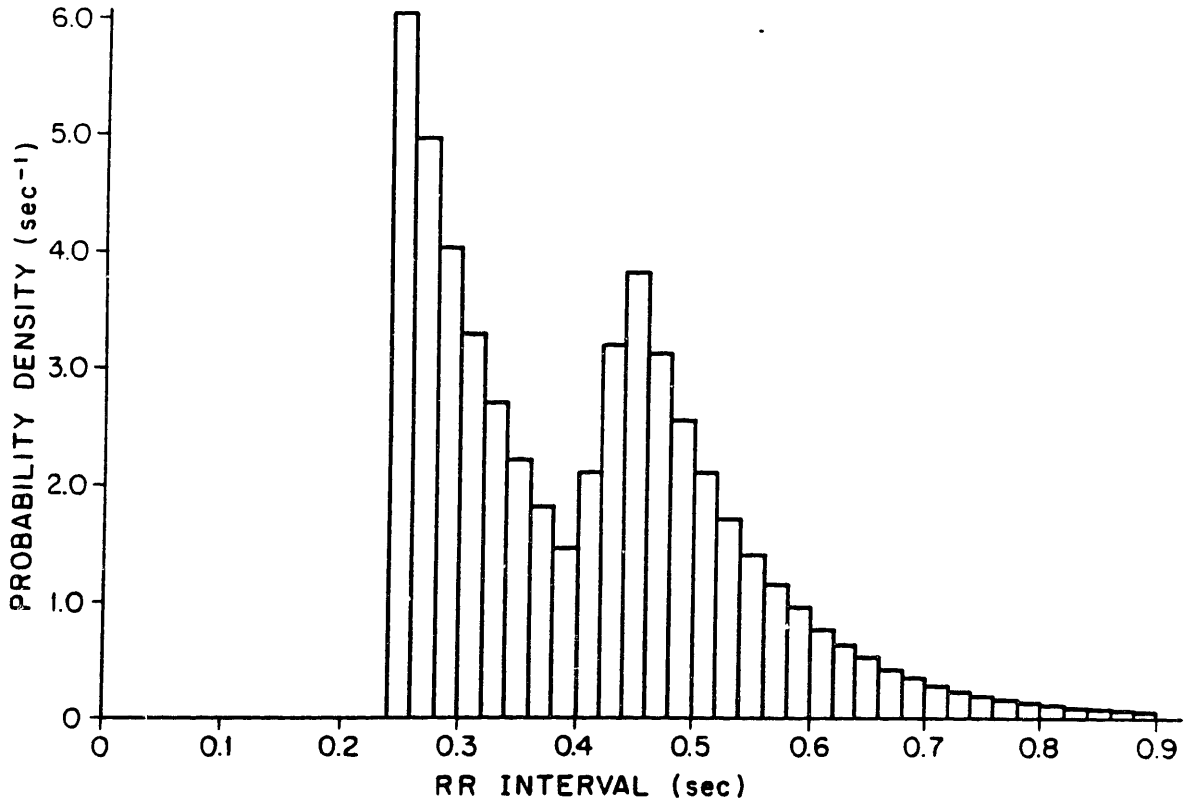

Figure 6.2: RR interval histogram predicted by the Moe and Abildskov model of atrial fibrillation depicted in Figure 6.1, where $\lambda = 10/\text{sec}$, $\tau_p = 0.20$ sec, and $\tau_d = 0.25$ sec. The initial large peak represents RR intervals that do not contain a 'concealed beat,' whereas the second peak (which actually overlaps on the first) results from RR intervals in which an atrial impulse arrived during the concealment zone. An analytical derivation of the form of the histogram appears in Appendix B.

histograms with multiple or narrow peaks cannot be accounted for by the Moe and Abildskov model of concealed conduction.

Honzikova *et al* [8] analyzed a variation of this model, although they presented it as that of Moe and Abildskov. In the concealed conduction model they considered, the AVJ functions as a single unit and can assume one of three possible states: absolutely refractory, relatively refractory, or fully excitable. When fully excitable, the AVJ would allow an atrial impulse to propogate through and evoke a ventricular beat. Such an event would also initiate a cycle in which the AVJ would become absolutely refractory for a time τ_a, and then become relatively refractory for a time τ_r. If a subsequent atrial impulse arrived while the AVJ were absolutely refractory, the impulse would be ignored. If, however, it arrived during the relatively refractory phase, the AVJ would not conduct the signal, thus 'concealing' the impulse, but a new cycle of an absolutely refractory period followed by a relatively refractory phase would begin anew (see Figure 6.3).

An RR interval histogram predicted by this model was presented by Honzikova *et al* [8]. Interestingly this model can predict a series of evenly spaced peaks in the histogram (see Appendix B and Figure 6.4). However, these peaks are all relatively broad and right skewed. Furthermore, the initial peak always begins with an abrupt step rise to its maximum value. The form of the predicted histogram therefore does not resemble that which is observed experimentally. Specifically, this model cannot explain the presence of narrow peaks superimposed on a smooth background as observed in the experimental RR interval histograms; nor can it account for the fact that most of the histograms rise slowly from the point $T = \tau$, rather than displaying an abrupt step increase.

Honzikova *et al* acknowledged that the histogram predicted by this model of concealed conduction was not satisfactory. As an alternative, they presented a model of atrial fibrillation in which atrial impulses arriving simultaneously at separate channels of the AVJ are summed. If this sum of electrical activity is sufficient, ventricular activation is initiated. This model, however, predicts solely unimodal histograms and thus, does not seem to adequately account for many of the statistical properties of the RR interval sequence often observed in atrial fibrillation patients. Similarly, the retarded excitation model of ten Hoopen [9] predicts unimodal histograms.

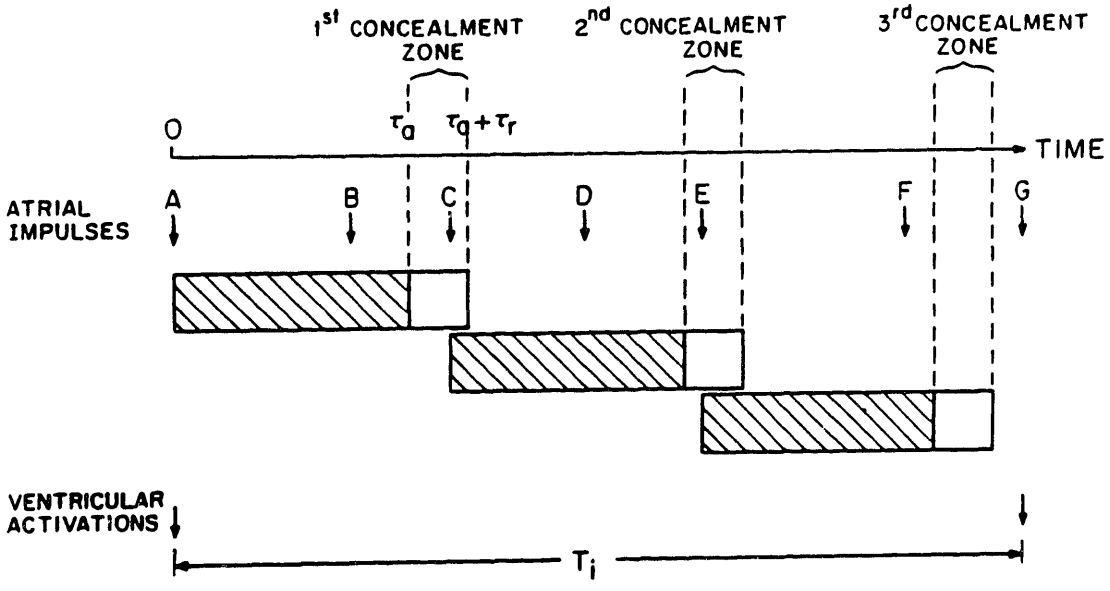

Figure 6.3: Schematic representation of the Honzikova *et al* [8] version of the 'concealed conduction' model for atrial fibrillation. In this model, the AVJ is represented by a single element in which a cycle of an absolutely refractory period followed by a relatively refractory period is initiated by a successfully propogated atrial impulse such as impulse A. If an impulse arrives when the AVJ is absolutely refractory, as is the case for impulses B, D, and F, then it is ignored. An impulse that arrives during the relatively refractory period, such as C and E, will initiate a new cycle of absolutely refractory and relatively refractory periods, but will not propogate through the AVJ and is thus 'concealed.' Note that unlike the Moe and Abildskov model [15] shown in Figure 6.1, this model predicts the possibility of second and even higher order concealment zones. Only when the AVJ is once again fully excitable can an atrial impulse traverse the AVJ and initiate a ventricular activation, as impulse G does.

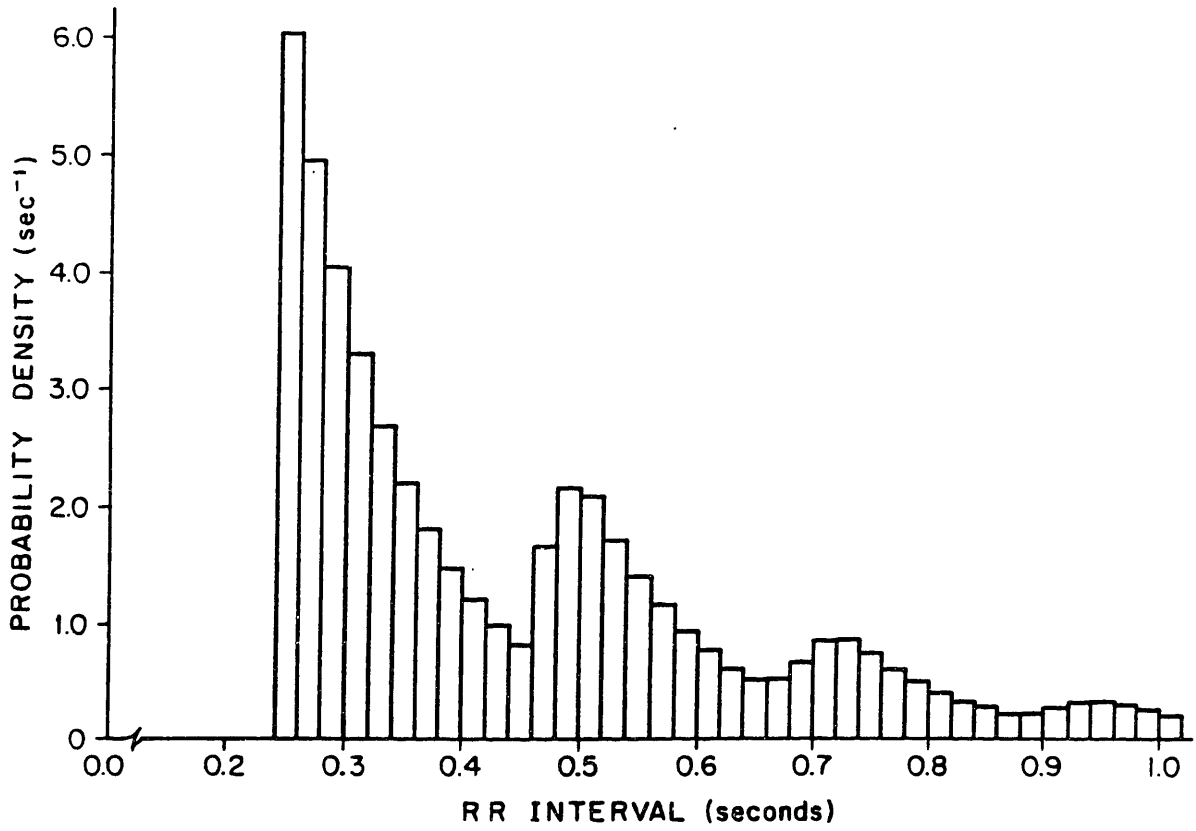

Figure 6.4: RR interval histogram predicted by the Honzikova *et al* version of the 'concealed conduction' model of atrial fibrillation shown in Figure 6.3. For this example, $\lambda = 10/\text{sec}$, $\tau_a = 0.20$ sec, and $\tau_r = 0.35$ sec. The histogram represents the superposition of a family of curves, where each successive curve results from the concealment of one more atrial impulse within the RR interval than the last curve. Thus the initial peak represents RR intervals in which no atrial impulses were concealed, the next peak represents intervals in which one impulse was concealed, etc. The exact form of the distribution is derived in Appendix B.

As a final point regarding concealed conduction, it is important to note that in the model presented in this thesis, as well, atrial impulses may enter the AVJ and not directly initiate a ventricular response. In this sense, the model presented here also includes a form of concealed conduction. But in this model, atrial impulses that arrive while the AVJ is excitable are summed and do not initiate a new refractory period until after the next ventricular activation has occurred.

Goldstein and Barnett [4] observed that many RR interval histograms of atrial fibrillation patients displayed an exponential tail. They explained that this phenomenon would be expected if a Poisson process were to describe the arrival of atrial events at the AVJ. The model presented in this thesis is consistent with that notion, except it should be pointed out that lower order Erlang functions, which are of the form $p(t)=\lambda(\lambda t)^n e^{-\lambda t}$, could easily be falsely recognized as pure exponentials. The technique they use for attempting to fit the logarithm of the histogram's tail with a straight line may not be sufficiently sensitive to distinguish between Erlangs and pure exponentials. There is a further similarity between the model presented in this thesis and that presented by Goldstein and Barnett, in that they also suggested that the AVJ undergoes a fully refractory period after each ventricular beat, during which atrial imput is ignored.

This concept of a fully refractory period was not considered, however, in the model presented by Hashida *et al* [5]. The other difference between their model and the one presented here is the inclusion here of a rate of spontaneous phase four depolarization. These workers, on the other hand, did recognize the Erlangian structure found in RR interval histograms of atrial fibrillation patients. In fact, the two models become identical in the special case of the model presented in this thesis where τ (the refractory period) and $\dot{V}_4$ (the rate of spontaneous depolarization) are both set to zero. The additional degrees of freedom afforded by the inclusion of these two parameters are necessary to explain (1) the apparent shift to the right of the beginning of the histograms, and (2) the presence of narrow peaks often seen superimposed on the Erlangian sections of the histogram.

Chapter 7

Conclusions

The model presented in this thesis successfully accounts for all the salient statistical features of the RR interval sequence. The four parameters of the model incorporate well documented and clinically accepted electrophysiologic features of the AVJ, and provide sufficient degrees of freedom to predict either unimodal or multiple-peaked histograms, depending on their values. Previous models of atrial fibrillation cannot account for the wide diversity of structures that the histograms may assume from one data record to another. Furthermore, the model of the atrioventricular junction equivalent cell presented here can also be used to simply explain AVJ function during normal sinus rhythm, Mobitz type I and Mobitz type II block.

This model may be useful in understanding a variety of clinical observations. For example, as was demonstrated in section 5.2, digitalis administration slows mean ventricular rate by reducing λ, the mean rate of arrival of atrial impulses at the AVJ, thereby decreasing the atrial contribution to the depolarization of the AVJEC. It is possible, however, that as digitalis dosage is increased the relative rate of phase four depolarization, $\dot{v}_4/(V_T - V_R)$, increases, causing a 'pseudoregularization' of the heart beat and a paradoxical increase in the mean ventricular rate. Thus, digitalis may convert the ventricular dysrhythmia from a highly irregular atrially controlled process to a more regular AVJ controlled process. The limiting case of the latter is junctional tachycardia often seen in the setting of digitalis toxicity.

The preliminary investiagation of this model indicates that it should be feasible to utilize the model to analyze a given RR interval sequence, and deduce the numerical maginitudes of some or all of the model's four parameters: the mean rate at which atrial impulses arrive at the AVJ, the relative amplitude of the impulses, the rate of spontaneous phase four depolarization of the AVJEC, and the refractory period of the AVJEC. Therefore, the potential exists to utilize these parameters as electrophysiologic indices to probe mechanisms of drug action, and perhaps to guide pharmacologic management of atrial fibrillation.

Appendix A

Mathematical Analysis of the Model

Inspection of the illustration of the model presented in this thesis (Figure 3.1) reveals the following expression for the transmembrane potential of the AVJ equivalent cell:

$$V_m = V_R + \dot{V}_4 \tilde{t} + n(\tilde{t})\Delta V \tag{A.1}$$

Here, V_m is the transmembrane potential, $\tilde{t}$ is the time elapsed since the end of the refractory period, V_R is the resting potential, $n(\tilde{t})$ is the number of atrial impulses that have arrived by time $\tilde{t}$, $\dot{V}_4$ is the spontaneous rate of phase four depolarization, and ΔV is the amplitude of the atrial impulses.

Since the arrival of atrial impulses at the AVJ is considered as a Poisson process, the single-time probability distribution, or histogram, for $n(\tilde{t})$ is given by:

$$p_n = \frac{e^{-\lambda \tilde{t}}(\lambda \tilde{t})^n}{n!} \tag{A.2}$$

where λ is the mean rate of arrival for the Poisson process. Note that $n(\tilde{t})$ must necessarily take on an integer value for all $\tilde{t}$.

The criterion for initiation of ventricular activation at time t is that $V_m = V_T$ where V_T is the threshold potential; setting $V_m = V_T$ and $t = \tilde{t}$ in equation A.1 gives the following expression:

$$V_T = V_R + \dot{V}_4 t + n(t)\Delta V \tag{A.3}$$

What we would like to determine is the probability distribution for t, the time elapsed since the end of the refractory period at which the transmembrane potential crosses the threshold level.

It is convenient to re-express equation A.3 using the new variables,

$$\nu = \dot{V}_4/\Delta V$$
$$N = (V_T - V_R)/\Delta V$$

The quantity ν is the rate of spontaneous phase four depolarization measured in units of ΔV. N is the number of atrial impulses required to depolarize the AVJEC to threshold in the absence of spontaneous phase four depolarization (*i.e.* when $\dot{V}_4 = 0$). In terms of these parameters, equation

A.3 becomes:

$$N = vt + n(t) \tag{A.4}$$

We may obtain an expression for the cumulative probability, $P_t(t)$, that the transmembrane potential reaches threshold at or before time t, as follows: $1 - P_t(t)$ is equal to the probability that the time required to reach threshold is greater than t. According to equation A.4, this could occur only if $n(t)$ is less than $N - vt$. The cumulative probability that $n(t) < N - vt$ may be obtained from equation A.2 by summing over all integer values of n less than $N - vt$:

$$1 - P_t(t) = \sum_{k=0}^{N-vt} \frac{e^{-\lambda t}(\lambda t)^k}{k!} \tag{A.5}$$

so that,

$$P_t(t) = 1 - \sum_{k=0}^{N-vt} \frac{e^{-\lambda t}(\lambda t)^k}{k!} \tag{A.6}$$

The sum extends over all integer values from zero up to, but not greater than, $N - vt$. Notice that $P_t(t)$ increases incrementally each time $N - vt$ is equal to an integer value. $P_t(t) = 0$ for $t < 0$, since t must be a positive number. $P_t(t) = 1$ for $t > N/v$ because N/v is the maximum time required to reach threshold, as this is the time it takes for the transmembrane potential to ramp from V_R to V_T.

We can compute the probability distribution $p_t(t)$ by differentiating $P_t(t)$ with respect to t:

$$\begin{aligned} p_t(t) &= \frac{dP_t(t)}{dt} \\ &= \frac{e^{-\lambda t}\lambda^{n+1}t^n}{n!} + \sum_{k=0}^{N-vt} \frac{e^{-\lambda t}(\lambda t)^k}{k!}\,\delta\left(t - \frac{N-k}{v}\right) \\ &\qquad \text{for} \quad 0 \le t \le N/v \end{aligned} \tag{A.7}$$

where n is the greatest integer less than $N - vt$, and $\delta(x)$ represents a delta function. Note that the first term of this expression describes an Erlang function of order n. Since n jumps from one integer to the next each time $(N - vt)$ takes on an integer value, the distribution described by $p_t(t)$ will include pieces of several different Erlang curves. The second set of terms in equation (A.7) represents a set of evenly spaced delta functions with various weights. The spacing between the delta functions is $\Delta t = 1/v$. It is precisely at the same points in time where the delta functions are

located that the semi-continuous component of $p_t(t)$ jumps from one Erlang curve to the next. Figure A.1 illustrates the superposition of the delta functions on the pieces of Erlang curves.

We now have calculated the probability distribution for the duration of phase four, $p_t(t)$. The probability distribution of RR intervals is easily obtained in the case where the refractory period, τ, is constant. The duration of the RR interval, T, is given by

$$T = t + \tau \tag{A.8}$$

Thus, the probability distribution for T is given by

$$p_t(T) = p_t(T - \tau) \tag{A.9}$$

If one shifts the theoretical histogram for t over to the right by an amount τ, one obtains the histogram for T. Figure A.2 shows a theoretical histogram calculated according to this model, under conditions where several peaks are evident.

It is interesting to examine the limit where $\nu = \dot{V}_4/\Delta V << \lambda$. In this case the weight of all the delta functions is very small, and equation A.7 approaches the limit

$$p_t(t) = \frac{e^{-\lambda t}\lambda^{\tilde{N}+1}t^{\tilde{N}}}{\tilde{N}!} \tag{A.10}$$

where $\tilde{N}$ corresponds to the greatest integer less than N. This solution corresponds to the case where only atrial impulses contribute to phase four depolarization. Such a distribution is plotted in Figure 2.2b. The Erlangian distribution obtained here, in the limit $\tau = 0$, corresponds to the distribution predicted by the model of Hashida *et al* [5].

In the opposite extreme limit, where $\nu = \dot{V}_4/\Delta V >> \lambda$, the delta function located at $t = N/\nu$ becomes very large (*i.e.* approaches an area of unity). In this case, $p_t(t)$ approaches simply

$$p_t(t) = \delta\left(t - \frac{N}{\nu}\right) \tag{A.11}$$

In this case, the spontaneous rate of phase four depolarization is the sole contributor to the increase in the transmembrane potential during phase four. The result is a perfectly regular set of RR intervals.

Note that variation in τ or $\dot{V}_4/(V_T - V_R)$ from one beat to the next, or in ΔV from one atrial

impulse to the next, will tend to broaden the delta functions in the histogram into peaks of finite width.

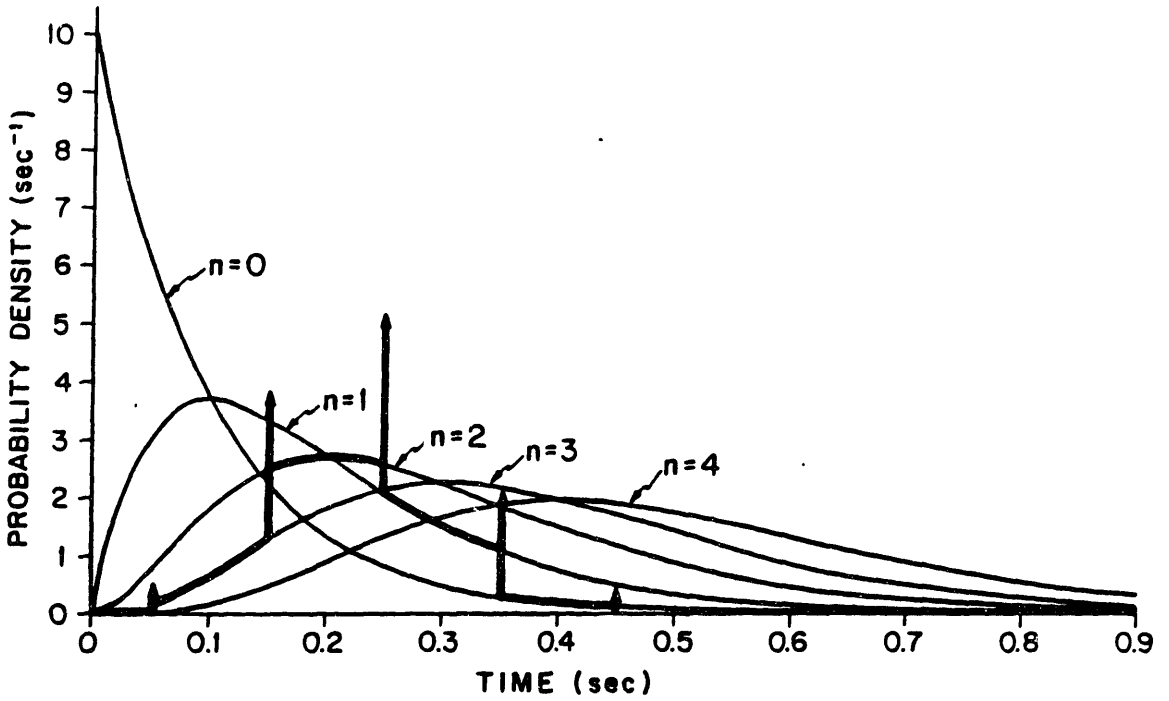

Figure A.1: Family of Erlang curves, *i.e.* $p_n(t) = \lambda e^{-\lambda t}(\lambda t)^n / n!$, for $\lambda = 10$/sec. The distribution for t, the duration of phase four, predicted by the AVJEC model includes pieces of Erlang curves with superimposed delta functoins at points where the distribution jumps from one Erlang to the next ($p_t(t)$ indicated by thick lines). In this example, $\Delta V/(V_T - V_R) = 0.222$ and $\dot{V}_4/(V_T - V_R) = 2.22$/sec.

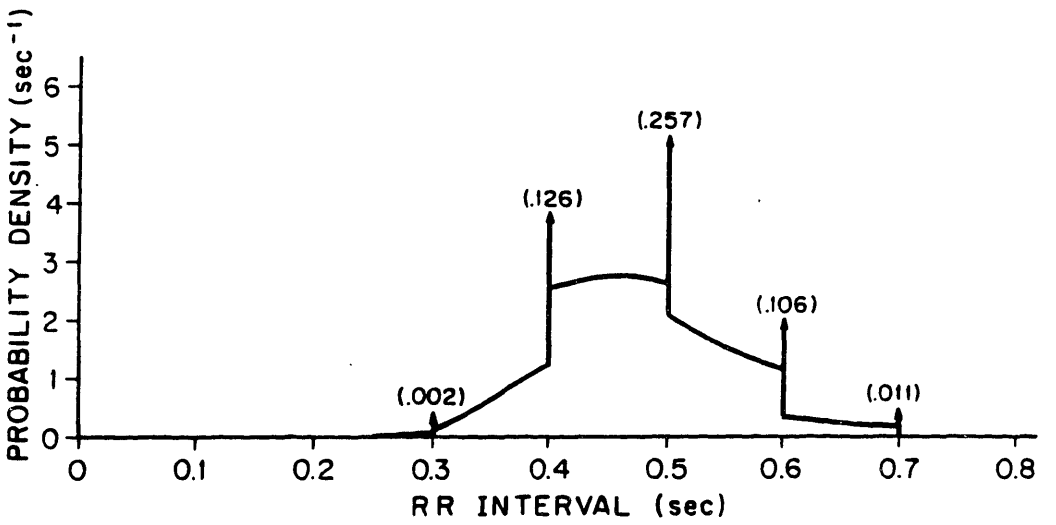

Figure A.2: RR interval histogram derived from distribution for phase four duration, t, shown in Figure A.1. Note that this distribution is identical to that for t except for a shift to the right by an amount $\tau = 0.25$ sec, corresponding to the refractory period. Numbers in parentheses are the weights of the delta functions.

Appendix B

Mathematical Analysis of Concealed Conduction Models of Atrial Fibrillation

§ B.1 Moe and Abildskov Model

According to the model of Moe and Abildskov [15], the AVJ is composed of a proximal region with refractory period τ_p and a distal portion with refractory period τ_d (see Figure 6.1). The AVJ is bombarded with impulses that arrive randomly in time with mean rate λ.

To simplify the analysis we will initially consider τ_p and τ_d to be constant, and not vary with the past history of the system. Furthermore, the analysis may be simplified by assuming an infinite conduction velocity through both regions of the AVJ. This does not introduce a new constraint, since the conduction velocity determines the delay between input and output of the AVJ, but is not a factor in determining the statistics of the RR interval sequence predicted by this model.

A time frame may be defined in which the last successfully conducted impulse (and thus, ventricular activation) occurs at time $T_0 = 0$. Now if $\tau_d < \tau_p$ then every successful activation of the proximal AVJ will also activate the distal AVJ. Therefore, the probability distribution of the RR interval, T, in this case would be simply:

$$p(T) = \lambda e^{-\lambda(T-\tau_p)} \quad \text{for } T > \tau_p \tag{B.1}$$

However, if $\tau_d > \tau_p$, the proximal AVJ may be activated one or more times before activation of the distal AVJ (and thus, the ventricle) occurs. Define T_n to be the time of the n^{th} successful activation of the proximal AVJ. The probability density for T_n when T_{n-1} is known (*i.e.*, conditional on T_{n-1}) is

$$p(T_n / T_{n-1}) = \lambda e^{-\lambda\left[T_n - (T_{n-1}+\tau_p)\right]} \quad \text{for } T_n > T_{n-1} + \tau_p \tag{B.2}$$

The joint probability distribution for all the successful activation times, $T_n, T_{n-1}, \ldots, T_1$, is

$$p(T_n, T_{n-1}, \ldots, T_1) = p(T_n, T_{n-1}, \ldots, T_1 / T_0=0)$$
$$= p(T_n / T_{n-1}) p(T_{n-1} / T_{n-2}) \ldots . p(T_1 / T_0=0)$$
$$= \lambda^n e^{-\lambda(T_n - n\tau_p)} \qquad \text{(B.3)}$$

for $T_n > T_{n-1} + \tau_p > T_{n-2} + 2\tau_p > \cdots > n\tau_p$

Let $p_n(T_n)$ designate the probability that the n^{th} activation of the proximal AVJ occurs at time T_n, and that this activation is the first activation to occur after time $T = \tau_d$. In this case T_n will also correspond to the time at which the distal AVJ is activated. $p_n(T_n)$ is evaluated as follows:

$$p_n(T_n) = \int_{(n-1)\tau_p}^{D} dT_{n-1} \int_{(n-2)\tau_p}^{T_{n-1}-\tau_p} dT_{n-2} \ldots .$$
$$\ldots . \int_{2\tau_p}^{T_3-\tau_p} dT_2 \int_{\tau_p}^{T_2-\tau_p} dT_1 \; p(T_n, T_{n-1}, \ldots, T_1)$$
$$= H(T_n - \tau_d) H(T_n - n\tau_p) \frac{\lambda e^{-\lambda(T_n - n\tau_p)} \left[\lambda(D - (n-1)\tau_p)\right]^{n-1}}{(n-1)!} \qquad \text{(B.4)}$$

where $D \equiv \text{minimum}(T - \tau_p, \tau_d)$

$$H(x) = \begin{cases} 0 & \text{if } x < 0 \\ 1 & \text{if } x > 0 \end{cases}$$

$n \leq n_0 + 1$

and

n_0 is the greatest integer less than τ_d / τ_p

Obviously, if $n \geq n_0 + 2 > \tau_d / \tau_p + 1$, then $p_n = 0$ since $T_{n-1} > (n-1)\tau_p > \tau_d$. Since T_{n-1} occurs after τ_d, in this case T_n cannot represent the time of the *first* impulse to arrive after τ_d. To obtain $p(T)$ we merely sum $p_n(T)$ over n:

$$p_n(T) = \sum_{n=1}^{n_0+1} p_n(T)$$
$$= e^{-\lambda T} \left[H(T - \tau_d) \lambda \sum_{k=0}^{n_0-1} e^{\lambda(k+1)\tau_p} \left\{\lambda(D - k\tau_p)\right\}^k / k! \right.$$
$$\left. + H\left\{T - (n_0+1)\tau_p\right\} \lambda e^{\lambda(n_0+1)\tau_p} \left\{\lambda(D - n_0\tau_p)\right\}^{n_0} / n_0! \right] \qquad \text{(B.5)}$$

Equation B.5 reveals an exponential time decay multiplied by a bracketed expression. The first term within the brackets represents a peak which begins at $T = \tau_d$; the second term within the brackets represents a peak which begins at $T = (n_0+1)\tau_p$. This distribution is illustrated in Figure

6.2.

Thus, the Moe and Abildskov model predicts a smooth exponential distribution with a single peak starting at $T = \tau_p$ when $\tau_p > \tau_d$, and a bimodal distribution when $\tau_p < \tau_d$. Allowing for beat-to-beat variations in τ_p and τ_d, the distribution indicated in equation B.5 may become smeared, but its essential features will not change.

§ B.2 Model of Honzikova et al

Honzikova *et al* presented the following model of concealed conduction [8] (which they in fact incorrectly attributed to Moe and Abildskov). In this model the AVJ is composed of a single element with an absolute refractory period τ_a and a relative refractory period τ_r (see Figure 6.3). The AVJ is totally unresponsive during the absolute refractory period; stimulation during the relative refractory period initiates a new absolute refractory period of duration τ_a, but does not activate the ventricles. Only a stimulation occurring after the relative refractory period will lead to ventricular activation. The AVJ is bombarded by atrial impulses randomly in time at a mean rate λ. We will once again ignore the finite time required for the impulse to transit through the AVJ (inasmuch as it does not affect the RR interval distribution).

Let $T = 0$ represent the time of the last successful activation of the ventricles. Let $p_n(T_n)$ represent the probability density that the n^{th} successful activation of the AVJ occurs at time T_n, and that this is the first activation of the AVJ to occur after the relative refractory period. In this case, T_n will also represent the time of ventricular activation. We can write T_n as the sum of n independent terms:

$$T_n = \Delta T_1 + \Delta T_2 + \cdots + \Delta T_n \qquad \text{(B.6)}$$

where $\Delta T_i = T_i - T_{i-1}$

For $1 \le i \le n-1$, ΔT_i is restricted to lie between τ_a and $\tau_a+\tau_r$; ΔT_n must be larger than $\tau_a+\tau_r$. We can now write p_n as a convolution of n functions:

$$p_n = f * f * f * \cdots * f * g \qquad \text{(B.7)}$$

The convolution includes $n-1$ f terms and one g term. $f(\Delta T_i)$ is the probability distribution for ΔT_i restricted to the range $\tau_a < \Delta T_i < \tau_a+\tau_r$; $g(\Delta T_i)$ represents the probability distribution for ΔT_i restricted to the range $\Delta T_i > \tau_a+\tau_r$:

$$f(\Delta T_i) = \lambda e^{-\lambda(\Delta T_i - \tau_a)} H(\Delta T_i - \tau_a) H(\tau_a+\tau_r-\Delta T_i) \qquad \text{(B.8)}$$

$$g(\Delta T_i) = \lambda e^{-\lambda(\Delta T_i - \tau_a)} H(\Delta T_i - \tau_a - \tau_r) \qquad \text{(B.9)}$$

$p_n(T_n)$ can be evaluated from equation B.7 using a Fourier Transform technique after substituting the sum of terms denoted in equation B.6 for T_n, to yield:

$$p_n(T_n) = \lambda e^{-\lambda(T_n - n\tau_a)} \sum_{m=0}^{n-1} \left[\frac{(-1)^m}{(n-1-m)!\, m!} \right]$$

$$\cdot \left[\lambda \left(T_n - n\tau_a - (m+1)\tau_r \right) \right]^{n-1} \cdot H\left(T_n - n\tau_a - (m+1)\tau_r \right) \qquad \text{(B.10)}$$

Each $p_n(T_n)$ is characterized by a single peak starting at $T = n\tau_a + \tau_r$. The complete probability distribution $p(T)$ for the RR interval is given simply by:

$$p(T) = \sum_{n=1}^{\infty} p_n(T_n) \qquad \text{(B.11)}$$

An example of such a distribution is shown in Figure 6.4.

Appendix C

Computer Program for Deduction of Model Parameters

In this appendix is shown the computer program written in BASIC used for the deduction of the four parameters of the model presented in this thesis. The program consists of three subprograms, AFIB3, AFIB4, and AFIB5. Upon completion of execution of AFIB3, control is passed to AFIB4 by the statement, "CHAIN AFIB4." Similarly, after complete execution of AFIB4, control is passed to AFIB5 via the "CHAIN AFIB5" statement. For a description of the algorithm implemented in this program, see section 4.4.

```
5 REM AFIB3
6 FOR J=1 TO 10
7 PRINT
8 NEXT J
10 PRINT 'ATRIAL FIBRILLATION ANALYSIS'
20 GOSUB 50
30 GO TO 100
50 PRINT
70 PRINT
80 RETURN
100 DIM #1,T%(1015)
105 COMMON C(1015),D(1015),E(1015),T(1015),U(1015)
110 COMMON F(2,40),R(200,4),K(30,3),X(10),S(9)
130 COMMON M,C0,C1,F9,F8,L1,L2,L3,L4
150 REM      SUBROUTINE FOR INPUT DATA
160 PRINT 'INPUT DATA FILE NAME';
163 F8=F8+1
164 FOR J=1 TO F8
165 READ A$
166 NEXT J
170 DATA 'A1','A2','A3','A4','A5','A6'
180 PRINT ': ';A$
190 OPEN A$ FOR INPUT AS FILE #1
205 PRINT 'INPUT 0 FOR:  STANDARD CORRECTION FACTOR  .001'
215 PRINT TAB(14);'PRINT FIRST AND LAST 20 POINTS'
220 F2=0
225 IF F2<>0 THEN  GO TO 260
230 LET Q=1.00000E-03
250 LET F3=20
255 GO TO 300
260 PRINT 'INPUT 1 TO PRINT RAW DATA'
265 PRINT TAB(6);'N FOR PRINT FIRST AND LAST N INPUT RAW DATA'
270 INPUT F3
275 PRINT 'INPUT DATA COR. FACTOR, 0 IS DEFAULT (.001)'
280 INPUT Q
285 IF Q<>0 THEN  GO TO 295
290 LET Q=1.00000E-03
292 LET D1=D
295 REM
300 PRINT 'INPUT 0 FOR ALL DEFAULTS'
305 F9=0
322 FOR J=1 TO 1015
324 LET C(J)=0
325 LET D(J)=0
326 NEXT J
330 IF F3<1 THEN  GO TO 340
335 PRINT '1';
340 FOR I9=1 TO 1010
342 T(I9)=T%(I9)
348 IF T(I9)=0 THEN 400
350 IF F3=1 THEN  GO TO 360
355 IF I9>F3 THEN  GO TO 380
360 PRINT T(I9);
365 IF INT(I9/5)-I9/5<-.1 THEN  GO TO 380
```

```
370 PRINT
375 PRINT I9+1;
380 REM
390 NEXT I9
400 LET M=I9
405 IF F3<1.5 THEN  GO TO 460
410 PRINT
415 LET I8=5*(INT((M-F3+1)/5)-1)
420 IF I8<1 THEN LET I8=1
425 PRINT I8+1;
430 FOR I9=I8+1 TO M
435 PRINT T(I9);
440 IF I9/5-INT(I9/5)>.1 THEN  GO TO 455
445 PRINT
450 PRINT I9+1;
455 NEXT I9
460 CLOSE #1
465 PRINT
470 PRINT 'NO. OF DATA POINTS INPUT IS=';M
472 GOTO 546
475 REM DC DRIFT CORRECTION
478 LET F4=0
480 LET X=0
482 LET S1=0
484 LET S2=0
486 LET S3=0
488 LET S4=0
490 FOR J=N0 TO N1
492 LET X=X+T(J)
494 LET S1=S1+X
496 LET S2=S2+X*T(J)
498 LET S3=S3+X*X
500 LET S4=S4+T(J)*T(J)
502 NEXT J
504 LET M9=(S2-S1*X/M)/(S3-S1*S1/M)
506 LET B9=(X-M9*S1)/M
508 LET R9=M9*SQR((S3-S1*S1/M)/(S4-X*X/M))
509 PRINT
510 PRINT 'MEAN','SLOPE','INTERCEPT','CORR. COEF.'
512 PRINT X/M,M9,B9,R9
514 PRINT
515 IF F4>.01 THEN RETURN
516 PRINT 'DO YOU WANT TO CORRECT FOR DC DRIFT';
517 RETURN
518 IF F9<.01 THEN  GO TO 524
520 INPUT F4
522 IF F4<.01 THEN RETURN
524 LET X0=(X/M-B9)/M9
526 LET X=0
528 FOR J=N0 TO N1
530 IF T(J)<.01 THEN  GO TO 536
532 LET X=X+T(J)
534 LET T(J)=T(J)-(X-X0)*M9
536 NEXT J
```

Portions of the text
on the following page(s)
are not legible in the
original.

```
642 LET F4=1
644 GO TO 480
646 IF F4<.01 THEN  GO TO 580
648 LET N0=5
650 LET N1=1005
652 GO TO 722
680 PRINT
685 PRINT 'INPUT 1 FOR PRINT ROUTINE, 0 FOR NO PRINT'
688 INPUT I
689 PRINT
690 IF I<.1 THEN  GO TO 605
695 GOSUB 880
600 GO TO 580
605 PRINT 'INPUT I FOR FIXPOINT NO. I OR 0 FOR NO FIXPOINT'
610 INPUT I
615 IF I>.5 THEN  GO TO 630
620 PRINT
625 GO TO 640
630 INPUT T(I)
635 GO TO 605
640 PRINT 'INPUT I FOR INSERT POINT NO. I OR 0 FOR NO INSERT'
645 INPUT I
650 IF I>.5 THEN  GO TO 655
652 PRINT
654 GO TO 695
655 LET T=J(I)
660 INPUT T(I)
665 FOR J=I TO M
670 LET T1=T(J+1)
675 LET T(J+1)=T
680 LET T=T1
685 NEXT J
690 LET M=M+1
692 GO TO 640
695 PRINT 'INPUT I FOR DELETE POINT NO. I OR 0 FOR NO DELETE'
698 INPUT I
700 IF I<.5 THEN  GO TO 710
705 LET T(I)=0
708 GO TO 695
710 PRINT
712 GOSUB 880
714 PRINT
715 PRINT 'INPUT FIRST AND LAST POINTS'
720 INPUT N0,N1
722 IF N1>M THEN LET N1=M-5
724 LET M=N1-N0+1
725 LET C0=1.00000E+36
730 LET C1=-C0
735 LET C=0
736 LET N2=0
740 FOR J=N0 TO N1
742 IF T(J)<1.00000E-03 THEN  GO TO 770
745 LET C=C+T(J)
747 LET N2=N2+1
```

```
750 IF T(J)<C1 THEN  GO TO 760
755 LET C1=T(J)
760 IF T(J)>C0 THEN  GO TO 770
765 LET C0=T(J)
770 NEXT J
775 LET C=C/N2
780 PRINT 'MEAN=';C;TAB(4);'LIMITS DEFINED BY .4*C, 1.6*C=';.4*C;1.6*C
785 LET I=0
788 PRINT 'POINTS FURTHER THAN .6 MEANS FROM MEAN:'
790 FOR J=N0 TO N1
792 IF T(J)<1.00000E-03 THEN  GO TO 810
795 IF ABS(T(J)-C)/C<.6 THEN  GO TO 810
800 PRINT J,T(J)
805 LET I=1
810 NEXT J
812 PRINT
815 IF I>.5 THEN  GO TO 822
820 PRINT 'NO POINTS MORE THAN .6 MEANS FROM THE MEAN FOUND'
822 IF F9<.01 THEN  GO TO 842
825 GOSUB 880
830 PRINT 'INPUT 1 FOR ANOTHER CYCLE OF CORRECTION, 0 FOR NO MORE'
835 INPUT I
840 IF I>.5 THEN  GO TO 605
842 GOSUB 475
845 FOR I=1 TO 1015
850 LET T(I)=T(I)*Q
855 NEXT I
860 LET C=C*Q
865 LET C0=C0*Q
870 LET C1=C1*Q
875 GO TO 962
880 REM SUBROUTINE TO PRINT
885 PRINT 'INPUT LOWER, UPPER LIMITS OF PRINT - OR 0,0 FOR NO PRINT'
890 INPUT M5,M6
895 IF M6=0 THEN  GO TO 960
900 LET M5=M5*INT((M5-1)/5)+1
905 IF M5<0 THEN LET M5=0
910 LET M6=5*(INT((M6-1)/5)+1)
915 IF M6>5*(INT(M/5)+1) THEN LET M6=5*(INT(M/5)+1)
920 PRINT M5;
925 FOR I9=M5 TO M6
930 PRINT T(I9);
935 IF I9/5-INT(I9/5)>.1 THEN  GO TO 955
940 PRINT
945 IF I9=M6 THEN  GO TO 955
950 PRINT I9+1;
953 NEXT I9
960 RETURN
962 LET C=0
964 LET D=0
965 LET M=0
966 FOR J=N0 TO N1-1
968 IF T(J)<1.00000E-03 THEN  GO TO 985
970 IF T(J+1)<1.00000E-03 THEN  GO TO 985
```

```
970 LET M=M+1
975 LET C(M)=T(J)
980 LET D(M)=T(J+1)
970 LET C=C+C(M)
990 LET D=D+D(M)
995 NEXT J
998 LET C=C/M
999 LET D=D/M
1000 REM SUBROUTINE TO COMPUTE TAU-INF.
1005 FOR I=1 TO 9
1010 LET S(I)=0
1015 NEXT I
1020 FOR I=1 TO M
1030 LET S(1)=S(1)+(D(I)-D)*(C(I)-C)
1035 LET S(2)=S(2)+C(I)*(C(I)-C)
1040 LET S(3)=S(3)+C(I)*C(I)*(C(I)-C)
1045 LET S(4)=S(4)+C(I)*C(I)*C(I)*(C(I)-C)
1050 LET S(9)=S(9)+(C(I)-C)*(C(I)-C)
1055 NEXT I
1056 FOR I=1 TO 9
1057 S(I)=S(I)/(M-1)
1058 NEXT I
1060 PRINT
1070 PRINT 'VARIANCE, S.D. =';S(9),SQR(S(9))
1072 PRINT '1ST AUTOCOR. TERM=';S(1);'=';S(1)/S(9);'* VARIANCE'
1074 GOTO 2500
1075 IF F9<.01 THEN  GO TO 1080
1076 PRINT
1077 PRINT 'DO YOU WANT TAU-INF. ROUTINE';
1078 INPUT Q
1079 IF Q<.01 THEN  GO TO 2500
1080 LET A(2)=S(3)/((S(2)-S(1))*2)
1085 LET Z3=A(2)/5
1090 PRINT
1095 PRINT 'TAU INF','INT. VAR.','STEP'
1100 LET A(1)=A(2)-Z3
1105 LET A(3)=A(2)+Z3
1110 FOR J=1 TO 3
1115 LET Z1=A(J)
1120 GOSUB 1400
1125 LET B(J)=V
1130 NEXT J
1135 LET M1=1.00000E+36
1140 LET M2=-M1
1145 FOR J=1 TO 3
1150 IF B(J)<M2 THEN  GO TO 1165
1155 LET M2=B(J)
1160 LET J2=J
1165 IF B(J)>M1 THEN  GO TO 1180
1170 LET M1=B(J)
1175 LET J1=J
1180 NEXT J
1185 IF M1=M2 THEN  GO TO 1240
1190 IF J2=2 THEN  GO TO 1240
```

```
1195 LET A(4-J2)=A(2)
1200 LET B(4-J2)=B(2)
1205 LET A(2)=A(J2)
1210 LET B(2)=B(J2)
1215 LET A(J2)=A(2)+(J2-2)*Z3
1220 LET Z1=A(J2)
1221 IF Z1>0 THEN  GO TO 1225
1222 LET Z3=Z3/2
1223 GO TO 1215
1225 GOSUB 1400
1230 LET B(J2)=V
1235 GO TO 1135
1240 REM
1242 IF Z3<.01 THEN  GO TO 1285
1245 LET Z3=Z3/2
1250 LET A(J1)=A(2)
1255 LET B(J1)=B(2)
1260 LET A(2)=A(1)+Z3
1265 LET Z1=A(2)
1270 GOSUB 1400
1275 LET B(2)=V
1280 GO TO 1135
1285 LET T1=A(2)
1288 PRINT
1290 PRINT "TAU-INF =";T1
1295 PRINT "INTRINSIC VARIANCE OF DATA =";-B(2)
1300 GO TO 2000
1400 REM  SUBROUTINE FOR CALCULATING INTRINSIC VARIANCE
1405 LET V=0
1410 LET W=0
1415 FOR I=1 TO M
1425 LET Z2=Z1*(1-EXP(-C(I)/Z1))
1430 LET U(I)=D(I)-Z2
1435 LET W=W+U(I)
1445 NEXT I
1450 LET W=W/M
1455 FOR I=1 TO M
1460 LET V=V+(U(I)-W)*(U(I)-W)/(M-1)
1465 NEXT I
1470 LET V=-V
1472 PRINT Z1,-V,Z3
1475 RETURN
2000 REM   SUBR. FOR CORRECTING FOR REFRACT. PERIODS
2025 LET U0=0
2035 FOR I=1 TO M
2040 LET U(I)=T1*(1-EXP(-C(I)/T1))
2045 LET U0=U0+U(I)/M
2050 NEXT I
2065 LET U3=0
2070 LET U4=1.00000E+36
2075 LET U5=-1.00000E+36
2080 FOR I=1 TO M
2085 LET U3=U3+(U(I)-U0)*(U(I)-U0)/(M-1)
2090 IF U(I)<U4 THEN LET U4=U(I)
```

```
2095 IF U(I)>U5 THEN LET U5=U(I)
2100 NEXT I
2105 LET D=0
2110 FOR I=1 TO M
2112 LET D(I)=D(I)-U(I)+U0
2115 LET D=D+D(I)/M
2120 NEXT I
2122 LET S(1)=0
2124 FOR I=1 TO M
2126 LET S(1)=S(1)+(D(I)-D)*(C(I)-C)/(M-1)
2128 NEXT I
2130 PRINT '1ST AUTOCOR. TERM AFTER CORRECTION =';S(1)
2131 PRINT TAB(35);'=';-S(1)/B(2);'*VARIANCE'
2132 PRINT
2134 PRINT 'REFRACTORY PERIOD STATISTICS:'
2135 PRINT TAB(10);'AVE/ VAR. S.D.=';U0;U3;SQR(U3)
2138 PRINT TAB(10);'MIN, MAX      =';U4;U5
2140 REM NEC TO RESET C0 AND C1
2142 LET C0=1.00000E+36
2145 LET C1=-C0
2150 FOR I=1 TO M
2155 IF D(I)<C0 THEN LET C0=D(I)
2160 IF D(I)>C1 THEN LET C1=D(I)
2165 NEXT I
2500 FOR J=1 TO 1015
2502 LET T(J)=0
2505 LET E(J)=0
2508 LET U(J)=0
2510 NEXT J
2515 FOR J=1 TO M
2520 LET S=INT((D(J)-C0)/(C1-C0)*999+1.5)
2525 LET E(S)=E(S)+1
2530 NEXT J
2535 LET I=1
2540 FOR J=1 TO 1000
2545 IF E(J)<.2 THEN  GO TO 2568
2550 LET T(I)=(J-1)*(C1-C0)/999+C0
2555 LET I=I+1
2560 LET E(J)=E(J)-1
2565 GO TO 2545
2568 LET U(J)=I-1
2570 NEXT J
2573 LET U(0)=0
2575 LET M=I-1
2595 CHAIN 'AFIB4'
```

```
2400 REM AFIB4
2401 COMMON C(1015),D(1015),E(1015),T(1015),U(1015)
2402 COMMON F(2,40),R(200,4),K(30,3),X(10),S(9)
2404 COMMON M,C0,C1,F9,F8,L1,L2,L3,L4
2408 REM INITIAL ESTIMATE AND MOMENT CALC.
2410 LET L1=0
2415 FOR J=1 TO M
2420 LET L1=L1+T(J)
2425 NEXT J
2427 L1=L1/M
2430 LET L2=0
2435 LET L3=0
2440 LET L4=0
2445 FOR J=1 TO M
2450 LET L=T(J)-L1
2455 LET L2=L2+L*L
2460 LET L3=L3+L*L*L
2465 LET L4=L4+L*L*L*L
2470 NEXT J
2472 L2=L2/(M-1)
2473 L3=L3/(M-1)
2474 L4=L4/(M-1)
2475 PRINT 'L1','L2','L3','L4'
2476 PRINT L1,L2,L3,L4
2477 PRINT
2479 Q=.02
2480 GOSUB 4400
2482 I8=10*INT(J/10+.9)
2484 Q=.98
2486 GOSUB 4400
2488 I9=10*INT(J/10)
2490 H(0)=1
2491 H(1)=0
2492 H(2)=L2
2493 H(3)=L3
2494 H(4)=L4
2500 REM SEARCH FOR LAMBDA,V,N,TAU
2505 PRINT 'LAMBDA','TAU','N','BETA','K      ERROR'
2508 Q9=.01
2510 Q=1-Q9
2512 GOSUB 4400
2514 T1=T
2516 E9=1000
2518 E8=0
2520 A(1)=0
2522 Q=.005
2524 GOSUB 4400
2525 A7=T
2526 A8=0
2527 A9=10
2528 GOTO 2535
2529 A8=2
2530 A9=6
2531 A(1)=X(4)-A7/10
```

```
2532 A(4)=X(4)+A7/10
2533 A(2)=.618*A(1)+.382*A(4)
2534 A(3)=.382*A(1)+.618*A(4)
2535 FOR A0=A8 TO A9
2536 IF E8=1 THEN 2539
2537 X(4)=A7*A0/10
2538 GOTO 2570
2539 IF A0>3 THEN 2542
2540 A1=A0
2541 GOTO 2564
2542 IF B(3)<B(2) THEN 2554
2543 A(4)=A(3)
2544 A(3)=A(2)
2546 B(3)=B(2)
2548 A(2)=A(1)+.382*(A(4)-A(1))
2550 A1=2
2552 GOTO 2564
2554 A(1)=A(2)
2556 A(2)=A(3)
2558 B(2)=B(3)
2560 A(3)=A(1)+.618*(A(4)-A(1))
2562 A1=3
2564 X(4)=A(A1)
2566 B(A1)=1000
2570 X9=(L1-X(4))/H(2)
2572 C(1)=0
2574 C(4)=X9
2576 C(2)=C(1)+.382*(C(4)-C(1))
2578 C(3)=C(1)+.618*(C(4)-C(1))
2580 FOR B0=2 TO 8
2582 IF B0>3 THEN 2588
2584 B1=B0
2586 GOTO 2612
2588 IF D(3)<D(2) THEN 2602
2590 C(4)=C(3)
2592 C(3)=C(2)
2594 D(3)=D(2)
2596 C(2)=C(1)+.382*(C(4)-C(1))
2598 B1=2
2600 GOTO 2612
2602 C(1)=C(2)
2604 C(2)=C(3)
2606 D(2)=D(3)
2608 C(3)=C(1)+.618*(C(4)-C(1))
2610 B1=3
2612 X(1)=C(B1)
2730 K(0,2)=T1-X(4)
2732 Q=1-Q9
2733 K(0,3)=Q
2735 T2=T1
2740 I=0
2745 Y=X(1)*(T2-X(4))
2748 F7=0
2750 GOSUB 5200
```

```
2752 F7=1
2755 IF P<Q THEN 2768
2760 I=I+1
2765 GO TO 2750
2768 F7=0
2770 K(0,1)=I-1
2772 K=1
2773 Q8=Q
2775 GOSUB 4900
2780 K(K,1)=I
2785 K(K,2)=D
2790 K(K,3)=Q
2795 IF F6>0 THEN 2812
2800 I=I+1
2805 K=K+1
2808 IF K>30 THEN 3124
2810 GO TO 2775
2812 K=K-1
2813 IF I<40 THEN 2816
2814 PRINT 'I =';I
2815 GOTO 3124
2816 D3=0
2818 IF K>0 THEN 2845
2820 I0=K(1,1)-1
2825 IF I0<0 THEN I0=0
2830 GOSUB 3215
2840 GOTO 2880
2845 IF K>1 THEN 2900
2850 I0=K(1,1)
2855 GOSUB 3272
2880 PRINT X(1),X(4),' ',' ',K;
2885 GOTO 3100
2900 A=0
2905 B=1-2*Q9
2910 C=0
2912 X=0
2913 Z=0
2915 FOR J=0 TO K
2920 IF K(J,1)>=0 THEN 2945
2930 N=0
2935 V=0
2940 GO TO 3025
2945 IF J>0 THEN 2980
2950 V=1/(K(1,2)-K(2,2))
2955 N=K(1,1)+K(1,2)*V
2960 IF (N-K(0,1))/V>=K(0,2) THEN 3025
2965 V=1/(K(0,2)-K(1,2))
2970 N=K(0,1)+K(0,2)*V
2975 GO TO 3025
2980 IF J<K THEN 3015
2985 V=1/(K(K-1,2)-K(K,2))
2990 N=K(K-1,1)+K(K-1,2)*V
2995 IF (N-K(K+1,1))/V<=K(K+1,2) THEN 3025
3000 V=1/(K(K,2)-K(K+1,2))
```

```
3005 N=K(K,1)+K(K,2)*V
3010 GO TO 3025
3015 V=1/(K(J,2)-K(J+1,2))
3020 N=K(J,1)+K(J,2)*V
3025 D=(K(J,2)+K(J+1,2))/2
3030 D2=(K(J,2)*K(J,2)+K(J,2)*K(J+1,2)+K(J+1,2)*K(J+1,2))/3
3035 P=K(J,3)-K(J+1,3)
3040 A=A+(N-V*D)*P
3045 C=C+D*P
3050 X=X+(N*D-V*D2)*P
3055 Z=Z+D2*P
3060 NEXT J
3065 X(3)=(X*C-A*Z)/(C*C-B*Z)
3070 X(2)=(B*X-A*C)/(C*C-B*Z)
3075 B8=X(1)/X(2)
3080 PRINT X(1),X(4),X(3),B8,K;
3100 GOSUB 5000
3102 PRINT E
3104 IF E8=2 THEN 3200
3106 D(B1)=E
3108 IF E8=0 THEN 3113
3110 IF E>B(A1) THEN 3120
3112 B(A1)=E
3113 IF E>E9 THEN 3120
3114 E9=E
3115 E(1)=X(1)
3116 E(4)=X(4)
3120 NEXT B0
3124 PRINT
3126 NEXT A0
3130 PRINT
3136 X(1)=E(1)
3138 X(4)=E(4)
3140 E8=E8+1
3142 IF E8=2 THEN 2730
3144 PRINT X(1),X(4)
3146 PRINT
3148 PRINT
3150 GOTO 2529
3200 REM OUTPUT
3205 PRINT
3207 PRINT K;"DELTA FUNCTIONS FOUND"
3208 PRINT
3210 IF K>0 THEN 3265
3212 PRINT "I =";I0
3213 GOSUB 3215
3214 GOTO 3335
3215 X(5)=1/(K(0,2)-K(K+1,2))
3220 X(6)=I0
3225 X(7)=I0+1+K(0,2)*X(5)
3230 X(2)=X(5)/2
3235 X(3)=I0+X(2)*K(0,2)
3240 X(8)=1/X(7)
3242 IF I0=0 THEN I0=1E-06
```

```
3245 X(9)=1/I0
3250 X(10)=X(5)/I0
3260 RETURN
3265 IF K=1 THEN 3400
3267 PRINT 'I','T(I)','P(I)'
3269 PRINT I0,K(1,2)+X(4),K(1,3)
3269 GOSUB 3272
3270 GOTO 3335
3272 X(5)=K(0,2)-K(1,2)
3275 IF K(1,2)-K(2,2)>X(5) THEN LET X(5)=K(1,2)-K(2,2)
3280 X(5)=1/X(5)
3285 X(6)=I0
3290 X(7)=I0+1+K(1,2)*X(5)
3295 IF I0+K(0,2)*X(5)<X(7) THEN LET X(7)=I0+K(0,2)*X(5)
3300 X(2)=X(5)/2
3305 X(3)=I0+X(2)*K(1,2)
3310 X(8)=1/X(7)
3312 IF I0=0 THEN I0=1E-06
3315 X(9)=1/I0
3320 X(10)=X(5)/I0
3325 RETURN
3335 PRINT
3340 GOSUB 4500
3345 PRINT 'LAMBDA','V','N','TAU','ERROR'
3350 PRINT X(1),'> 0','>';X(6),X(4),E
3355 PRINT ' ','<';X(5),'<';X(7)
3360 PRINT ' ','(';X(2);')','(';X(3);')'
3365 PRINT
3370 PRINT 'DELTA V / (V(T)-V(R))','>';X(8),'<';X(9)
3375 PRINT '(D V4 / D T) / (V(T)-V(R))','> 0','<';X(10)
3380 GO TO 5762
3400 X(5)=1/X(3)
3405 X(6)=X(2)/X(3)
3410 PRINT 'I','T(I)','P(I)'
3415 FOR J=0 TO K+1
3420 PRINT K(J,1),K(J,2)+X(4),K(J,3)
3425 NEXT J
3430 PRINT
3435 GOSUB 4500
3440 PRINT 'LAMBDA','V','N','TAU','ERROR'
3445 PRINT X(1),X(2),X(3),X(4),E
3450 PRINT
3455 PRINT 'DELTA V / (V(T)-V(R))','=';X(5)
3460 PRINT '(D V4 / D T) / (V(T)-V(R))','=';X(6)
3465 GO TO 5762
4300 REM SUBROUTINE FOR INTERPOLATION OF P-EXPT.
4305 IF T>C0-(C1-C0)/(2*999) THEN  GO TO 4320
4310 LET Q=0
4315 RETURN
4320 IF T<C1+(C1-C0)/(2*999) THEN  GO TO 4335
4325 LET Q=1
4330 RETURN
4335 LET J1=(T-C0)/(C1-C0)*999+.5
4340 LET J2=INT(J1)
```

```
4345 LET Q=((J1-J2)*U(J2+1)+(J2+1-J1)*U(J2))/M
4350 RETURN
4400 REM SUBROUTINE FOR INTERPOLATION OF T
4402 IF Q=0 THEN LET Q=1.00000E-06
4404 IF Q=1 THEN LET Q=.999999
4405 LET B9=0
4406 LET T9=T(INT(Q*M+.5))
4408 LET J=INT((T9-C0)/(C1-C0)*999+1.5)
4410 IF U(J)/M<Q THEN  GO TO 4435
4412 LET J=J-1
4414 GO TO 4410
4415 IF U(J)/M>Q THEN  GO TO 4455
4418 IF U(J)/M<Q THEN  GO TO 4435
4420 IF U(J)/M>S1 THEN  GO TO 4435
4425 LET B9=1
4430 GO TO 4445
4435 LET S1=U(J)/M
4440 LET T9=(J-.5)*(C1-C0)/999+C0
4445 LET J=J+1
4450 GO TO 4415
4455 LET J=J-B9
4460 LET S2=U(J)/M
4465 LET T8=(J-.5)*(C1-C0)/999+C0
4470 IF S1<>S2 THEN  GO TO 4485
4475 LET T=(T9+T8)/2
4480 RETURN
4485 LET T=(Q-S1)/(S2-S1)*T8+(S2-Q)/(S2-S1)*T9
4490 RETURN
4500 REM SUBROUTINE FOR CALCULATION OF ERROR FUNCTION
4501 I7=I8
4502 T=(I7-.5)*(C1-C0)/999+C0
4503 GOSUB 4700
4504 IF P<.02 THEN 4508
4505 I7=I7-10
4506 GO TO 4502
4508 LET E2=0
4509 LET E4=0
4510 LET E=0
4511 LET Q7=0
4512 LET I=INT(X(3))
4513 LET Y=X(1)*(X(3)-I)/X(2)
4514 GOSUB 5200
4515 LET E4=E4+F2
4516 LET P3=P-F3
4518 LET P4=P+F3
4520 FOR J=I7 TO I9 STEP 10
4522 Q=0
4524 IF J<1 THEN 4530
4525 LET Q=U(J)/M
4530 LET T=(J-.5)*(C1-C0)/999+C0
4542 IF I<0 THEN  GO TO 4570
4544 IF Q<P3 THEN  GO TO 4570
4546 IF Q>P4 THEN  GO TO 4552
4548 LET E1=0
```

```
4550 GO TO 4610
4552 LET I=I-1
4553 IF I<0 THEN  GO TO 4570
4554 LET Y=X(1)*(X(3)-I)/X(2)
4556 GOSUB 5200
4558 LET E4=E4+F2
4560 LET P3=P-F3
4562 LET P4=P+F3
4565 GO TO 4544
4570 GOSUB 4700
4575 IF P<1.5 THEN  GO TO 4605
4580 PRINT "OVERFLOW:  INT(N-VT) =";N
4585 LET E=1.00000E+30
4590 GO TO 4645
4605 LET E1=M*(P-Q)*(P-Q)/((Q*(1-Q))+(P*(1-P)))*2
4610 LET E3=E1
4615 IF E2<E1 THEN LET E3=E2
4620 LET E=E+E3*(Q-Q7)
4625 LET E2=E1
4628 LET Q7=Q
4630 NEXT J
4635 LET E=E+E4
4645 RETURN
4700 REM SUBROUTINE FOR CALCULATION OF P-THEORY
4702 LET P=0
4705 LET Z=0
4710 IF T-X(4)<0 THEN RETURN
4715 FOR K9=1 TO 3
4720 IF X(K9)>=0 THEN  GO TO 4730
4722 LET P=2
4725 LET Z=Z+1
4730 NEXT K9
4735 IF Z>.5 THEN RETURN
4750 LET Y=X(1)*(T-X(4))
4751 IF Y<80 THEN 4755
4752 E5=0
4753 GOTO 4800
4755 LET E5=EXP(-Y)
4760 LET F1=1
4770 LET N=INT(X(3)-X(2)*(T-X(4)))
4771 IF N<50 THEN  GO TO 4775
4772 P=2
4773 RETURN
4775 FOR K9=0 TO N
4780 LET P1=F1
4785 LET P=P+F1
4790 LET F1=F1*Y/(K9+1)
4795 NEXT K9
4800 LET P=1-E5*P
4805 LET P1=P1*E5*X(1)
4810 RETURN
4900 REM SUBROUTINE TO LOCATE EXP. DELTA FUNCTIONS.
4902 REM INPUT: I,T2,Q8,X(1),X(4),Q9
4903 REM OUTPUT: D,Q,F6,Q8,T2
```

```
4905 IF K=1 THEN 4925
4910 Q=Q8
4913 T=T2
4915 F=X(1)*(T-X(4))
4918 GOSUB 5200
4920 IF P>Q THEN 4950
4925 P2=P
4926 Q8=Q
4928 T2=T
4930 IF Q<Q9+5.00000E-03 THEN 4975
4935 Q=Q-.01
4940 GOSUB 4400
4945 GO TO 4915
4950 D=T-X(4)+(Q-P)/(P2-P-.01)*(T2-T)
4955 T=D+X(4)
4960 GOSUB 4300
4965 REM RETURNS Q
4968 F6=0
4970 RETURN
4975 D=T-X(4)
4980 Q=Q9
4985 F6=1
4990 RETURN
5000 REM SUBROUTINE FOR CALC. OF ERROR BY AREA
5002 I7=I8
5004 T=(I7-.5)*(C1-C0)/999+C0
5006 GOSUB 4700
5008 IF P<.02 THEN 5014
5010 I7=I7-10
5012 GOTO 5004
5014 E3=0
5015 E4=0
5016 FOR J=I7 TO I9 STEP 10
5018 Q=0
5020 IF J<1 THEN 5024
5022 Q=U(J)/M
5024 T=(J-.5)*(C1-C0)/999+C0
5026 GOSUB 4700
5028 E1=SQR(M*(P-Q)*(P-Q))
5030 E2=SQR(Q*(1-Q))
5032 E3=E3+E1
5034 E4=E4+E2
5036 NEXT J
5038 E=E3/E4
5040 RETURN
5200 REM SUBROUTINE TO CALCULATE P T,K (X(1)*T)
5202 IF F7=0 THEN 5208
5203 P1=P1+F3+F1
5204 F3=F1
5205 F1=F1*Y/(I+1)
5206 GOTO 5275
5208 LET P=0
5209 P1=0
5210 LET F1=1
```

```
5212 LET F2=0
5215 LET F3=0
5216 IF Y<0 THEN RETURN
5217 IF Y<80 THEN 5220
5218 E5=0
5219 GOTO 5265
5220 LET E5=EXP(-Y)
5225 FOR L=0 TO I
5240 LET F2=F1
5245 IF L=I THEN LET F1=F1/2
5250 LET P1=P1+F1
5252 F3=F1
5255 LET F1=F1*Y/(L+1)
5260 NEXT L
5262 LET F1=E5*F1
5265 LET F2=E5*F2
5270 LET F3=E5*F3
5272 LET P1=E5*P1
5275 LET P=1-P1
5280 RETURN
5762 CHAIN 'AFIB5'
```

```
2600 REM AFIB5
2601 COMMON C(1015),D(1015),E(1015),T(1015),U(1015)
2602 COMMON F(2,40),R(200,4),K(30,3),X(10),S(9)
2604 COMMON M,C0,C1,F9,F8,L1,L2,L3,L4
2700 GOTO 5762
4300 REM SUBROUTINE FOR INTERPOLATION OF P-EXPT.
4305 IF T<C0-(C1-C0)/(2*999) THEN  GO TO 4320
4310 LET Q=0
4315 RETURN
4320 IF T>C1+(C1-C0)/(2*999) THEN  GO TO 4335
4325 LET Q=1
4330 RETURN
4335 LET J1=(T-C0)/(C1-C0)*999+.5
4340 LET J2=INT(J1)
4345 LET Q=((J1-J2)*U(J2+1)+(J2+1-J1)*U(J2))/M
4350 RETURN
4400 REM SUBROUTINE FOR INTERPOLATION OF T
4402 IF Q=0 THEN LET Q=1.00000E-06
4404 IF Q=1 THEN LET Q=.999999
4405 LET B9=0
4406 LET T9=T(INT(Q*M+.5))
4408 LET J=INT((T9-C0)/(C1-C0)*999+1.5)
4410 IF U(J)/M<Q THEN  GO TO 4435
4412 LET J=J-1
4414 GO TO 4410
4415 IF U(J)/M>Q THEN  GO TO 4455
4418 IF U(J)/M<Q THEN  GO TO 4435
4420 IF U(J)/M>S1 THEN  GO TO 4435
4425 LET B9=1
4430 GO TO 4445
4435 LET S1=U(J)/M
4440 LET T9=(J-.5)*(C1-C0)/999+C0
4445 LET J=J+1
4450 GO TO 4415
4455 LET J=J-B9
4460 LET S2=U(J)/M
4465 LET T8=(J-.5)*(C1-C0)/999+C0
4470 IF S1<>S2 THEN  GO TO 4485
4475 LET T=(T9+T8)/2
4480 RETURN
4485 LET T=(Q-S1)/(S2-S1)*T8+(S2-Q)/(S2-S1)*T9
4490 RETURN
4700 REM SUBROUTINE FOR CALCULATION OF P-THEORY
4702 LET P=0
4705 LET Z=0
4710 IF T-X(4)<0 THEN RETURN
4715 FOR K9=1 TO 3
4720 IF X(K9)>=0 THEN  GO TO 4730
4722 LET P=2
4725 LET Z=Z+1
4730 NEXT K9
4735 IF Z>.5 THEN RETURN
4750 LET Y=X(1)*(T-X(4))
4751 IF Y<80 THEN 4755
```

```
4752 E5=0
4753 GOTO 4800
4755 LET E5=EXP(-Y)
4760 LET F1=1
4770 LET N=INT(X(3)-X(2)*(T-X(4)))
4771 IF N<50 THEN  GO TO 4775
4772 P=2
4773 RETURN
4775 FOR K9=0 TO N
4780 LET P1=F1
4785 LET P=P+F1
4790 LET F1=F1*Y/(K9+1)
4795 NEXT K9
4800 LET P=1-E5*P
4805 LET P1=P1*E5*X(1)
4810 RETURN
5762 IF X(2)<1.00000E-03 THEN  GO TO 5815
5765 PRINT
5780 PRINT 'A-V NODE PERIOD =',X(3)/X(2)+X(4)
5785 LET J=0
5790 LET T=(X(3)-J)/X(2)+X(4)
5795 PRINT 'PEAK AT T=',T
5800 LET J=J+1
5805 IF J>INT(X(3)) THEN  GO TO 5815
5810 GO TO 5790
5815 PRINT
5820 PRINT '            EXPERIMENTAL T STATISTICS'
5825 PRINT 'TMIN=';T(1),'TMAX =';T(M)
5830 PRINT 'MEAN HR =';60/L1
5835 PRINT 'MEAN','S.D.','SKEW','KURT'
5840 PRINT L1,SQR(L2),L3/L2^1.5,L4/L2/L2-3
5842 IF Y0>1.00000E+29 THEN  GO TO 5988
5845 L5=0
5850 LET T8=.01
5855 LET P=0
5860 LET J=1
5865 LET P0=P
5870 LET T=T8*J
5875 GOSUB 4700
5880 IF T<T(M) THEN  GO TO 5895
5885 IF P<.999 THEN  GO TO 5895
5890 GO TO 5910
5895 LET L5=L5+(T-T8/2)*(P-P0)
5900 LET J=J+1
5905 GO TO 5865
5910 LET L6=0
5915 LET L7=0
5920 LET L8=0
5925 LET P0=0
5930 FOR I=1 TO J-1
5935 LET T=T8*I
5940 LET L=(T-T8/2)-L5
5945 GOSUB 4700
5950 LET L6=L6+L*L*(P-P0)
```

```
5955 LET L7=L7+L*L*L*(P-P0)
5960 LET L8=L8+L*L*L*L*(P-P0)
5965 LET P0=P
5970 NEXT I
5972 PRINT
5975 PRINT '          THEORETICAL T STATISTICS'
5978 PRINT 'MEAN HR =';60/L5
5980 PRINT 'MEAN','S.D.','SKEW','KURT'
5985 PRINT L5,SQR(L6),L7/L6^1.5,L8/L6/L6-3
5988 PRINT
5990 PRINT '               PROBABILITY DISTRIBUTION'
6000 PRINT 'INPUT RANGE OF HISTOGRAM.'
6005 PRINT 'DEFAULT (0,0) IS 0, 1.1*TMAX.'
6008 IF F9<.01 THEN  GO TO 6020
6010 INPUT S1,S2
6015 IF S1+S2>.01 THEN  GO TO 6035
6020 LET S1=0
6030 LET S2=1.1*T(M)
6035 PRINT 'INPUT STEP SIZE, DEFAULT (0) IS .01, .02, OR .025 SEC.'
6038 IF F9<.01 THEN  GO TO 6050
6040 INPUT S3
6045 IF S3>1.00000E-05 THEN  GO TO 6055
6050 LET S3=.01
6052 IF S2-S1>.8 THEN LET S3=.02
6053 IF S2-S1>1.5 THEN LET S3=.025
6055 PRINT 'T','P-THEORY','P-EXPT.','IP-THEORY','IP-EXPT.'
6060 LET R=0
6065 LET R(0,3)=0
6070 LET R(0,4)=0
6075 FOR J=1 TO (S2-S1)/S3+1.5
6080 LET T=S1+(J-1)*S3
6085 GOSUB 4300
6090 LET R(J,2)=Q-R(J-1,4)
6095 LET R(J,4)=Q
6100 IF Y0<1.00000E+29 THEN  GO TO 6120
6105 LET R(J,1)=0
6110 LET R(J,3)=0
6115 GO TO 6138
6120 GOSUB 4700
6125 IF P<1.00000E-06 THEN LET P=0
6128 IF P>1.5 THEN LET P=0
6130 LET R(J,1)=P-R(J-1,3)
6135 LET R(J,3)=P
6136 IF R(J,1)>R THEN LET R=R(J,1)
6138 IF R(J,2)>R THEN LET R=R(J,2)
6140 PRINT T,R(J,1),R(J,2),R(J,3),R(J,4)
6175 NEXT J
6200 REM HISTOGRAMS, CUM. PROB. PLOTS
6202 PRINT
6204 PRINT
6205 PRINT 'HISTOGRAMS: T=THEORY, E=EXPT., X=BOTH'
6210 PRINT
6215 PRINT 'ENTER Y-MAX, DEFAULT (0) IS 1.1*P(MAX) =';1.1*R
6218 IF F9<.01 THEN  GO TO 6230
```

```
6220 INPUT P5
6225 IF P5>.01 THEN  GO TO 6235
6230 LET P5=1.1*R
6235 LET I=0
6240 GOSUB 6400
6245 PRINT 'CUM. PROB.: T=THEORY, E=EXPT., X=BOTH'
6250 PRINT
6255 PRINT TAB(30);'Y-MAX = 1'
6260 LET P5=1
6265 LET I=2
6270 GOSUB 6400
6275 PRINT 'DO YOU WANT TO REPLOT?';
6278 IF F9=0 THEN 6350
6280 INPUT Q
6285 IF Q<.1 THEN 6350
6288 LET F9=1
6290 PRINT 'DO YOU WANT TO CHANGE RANGE AND STEP SIZE?';
6295 INPUT Q
6300 IF Q>.1 THEN  GO TO 6000
6305 GO TO 6200
6350 CHAIN 'AFIB3'
6400 REM PLOTTING ROUTINE
6405 PRINT
6410 PRINT TAB(10);'|----+----+----+----+----+';
6415 PRINT '----+----+----+----+----+'
6420 FOR J=1 TO (S2-S1)/S3+1.5
6425 LET T=S1+(J-1)*S3
6426 LET T1=.1
6428 IF S3<.01 THEN LET T1=.01
6430 IF ABS(T-INT(T/T1+.5)*T1)>S3/2 THEN  GO TO 6438
6435 PRINT INT(T/T1+.5)*T1;TAB(9);'+';
6437 GO TO 6440
6438 PRINT TAB(9);'|';
6440 LET S(1)=INT(R(J,1+I)/P5*50+.5)
6445 LET S(2)=INT(R(J,2+I)/P5*50+.5)
6450 LET S(3)=S(1)
6455 LET S(4)=S(2)
6460 IF S(2)<S(1) THEN LET S(3)=S(2)
6465 IF S(2)<S(1) THEN LET S(4)=S(1)
6470 IF S(3)<=50 THEN  GO TO 6485
6475 PRINT TAB(60);'*'
6480 GO TO 6540
6485 PRINT TAB(10+S(3));
6490 IF S(4)-S(3)>.5 THEN  GO TO 6495
6492 PRINT 'X'
6493 GO TO 6540
6495 IF S(3)=S(1) THEN PRINT 'T';
6500 IF S(3)=S(2) THEN PRINT 'E';
6505 IF S(4)<=50 THEN  GO TO 6520
6510 PRINT TAB(60);'*'
6515 GO TO 6540
6520 PRINT TAB(10+S(4));
6530 IF S(4)=S(1) THEN PRINT 'T'
6535 IF S(4)=S(2) THEN PRINT 'E'
```

```
6340 NEXT J
6345 PRINT TAB(10);"|----+----+----+----+----+";
6350 PRINT "----+----+----+----+----+"
6355 FOR J=1 TO 5
6360 PRINT
6365 NEXT J
6370 RETURN
```

References

1. Akselrod S., Gordon D., Ubel F.A., Shannon D.C., Barger A.C., Cohen R.J.
   Power spectrum analysis of heart rate fluctuation: a quantitative probe of beat-to-beat cardiovascular control.
   Science 213: 220-222, 1981.

2. Arnoldi W.
   Die Ermittlung von dominierenden Rhythmen sowie der Schere der Rhythmusstörung bei Kranken mit Arhythmia perpetua.
   Klinische Wochenschrift 6: 1846-1848, 1927.

3. Bootsma B.K., Hoelen A.J., Strackee J., Meijler F.L.
   Analysis of RR intervals in patients with atrial fibrillation at rest and during exercise.
   Circulation 41: 783-794, 1970

4. Goldstein R.E., Barnett G.O.
   A statistical study of ventricular irregularity of atrial fibrillation.
   Computers and Biomed. Res. 1: 146-161, 1967

5. Hashida E., Yoshitani N., Tasaki T.
   A study on the irregularity of the sequence of R-R intervals in chronic atrial fibrillation in man based on the time series analysis and the information theory.
   Japenese Heart J. 19: 839-851, 1978

6. Hoff H.E., Geddes L.A.
   The respiratory-heart rate response in atrial fibrillation.
   Cardiovascular Res. Center Bulletin 4: 54-64, 1965

7. Hoff H.E., Geddes L.A.
   An analysis of the relationslhip between respiration and heart rate in atrial fibrillation.
   Cardiovascular Research Bulletin 4: 81-95, 1966

8. Honzikova N., Fiser B., Semrad B.
   Ventricular function in patients with atrial fibrillation.
   Cor. Vasa. 15: 257-264, 1973

9. Hoopen M. ten
   Ventricular response in atrial fibrillation
   Circulation Res. 19: 911-916, 1966

10. Horan L.G, Kistler J.C.
    Study of ventricular response in atrial fibrillation.
    Circulation Res. 9: 305-311, 1961

11. Jennings J.R., Stringfellow J.C., Graham M.
    A comparison of the statistical distributions of beat-by-beat heart rate and heart period.
    Psychophysiology 11: 207-210, 1974

12. Jordan H.
    Die zeitlichen Schwankungen der Herzschlagintervalle bei absoluter arrhythmie.
    Arch. Kreislaufforschung 21: 40-49, 1954

13. Langendorf R.
    Concealed A-V conduction: the effect of blocked impulses on the formation and conduction of subsequent impulses.
    Am. Heart J. 35: 542-552, 1948

14. Mendez C., Gruhzit C.C., Moe G.K.
    Influence of cycle length upon refractory period of auricles, ventricles, and A-V node in the dog.

Am. J. Physiol. 184: 287-295, 1956

15. Moe G.K., Abildskov J.A.
Observations on the ventricular dysrhythmia associated with atrial fibrillation in the dog heart.
Circulation Res. 14: 447-460, 1964

16. Söderström N.
What is the reason for the ventricular arrhythmia in cases of auricular fibrillation?
Am. Heart J. 40: 212-223, 1950

17. Urbach J.R., Grauman J.J., Straus S.H.
Quantitative methods for the recognition of atrioventricular junctional rhythms in atrial fibrillation.
Circulation 39: 803-817, 1969

18. Whittington J.R., Cross M.R., Raftery E.B.
An effective conscious animal model of atrial fibrillation.
Cardiovascular Res. 13: 105-112

19. Zipes D.P., Mendez C., Moe, G.K.
Evidence for summation and voltage dependency in rabbit atrioventricular nodal fibers.
Circulation Res. 32: 170-177, 1973